

AE Ursae Majoris – a δ Scuti Star in the Hertzsprung Gap

Jia-Shu Niu ^{1,2,3}, Jian-Ning Fu ¹¹, Yan Li ⁴, Xiao-Hu Yang ^{1,5}, Weikai Zong^{1,6,7}, Hui-Fang Xue ¹, Yan-Ping Zhang ¹, Nian Liu ¹, Bing Du ⁵ and Fang Zuo⁵.

¹*Astronomy Department, Beijing Normal University, Beijing 100875, P.R.China*

²*CAS Key Laboratory of Theoretical Physics and Kavli Institute for Theoretical Physics China (KITPC), Institute of Theoretical Physics, Chinese Academy of Sciences, Beijing, 100190, P.R.China*

³*School of Physical Sciences, University of Chinese Academy of Sciences, No.19A Yuquan Road, Beijing 100049, P.R.China*

⁴*National Astronomical Observatories/Yunnan Observatory, Chinese Academy of Sciences, PO Box 110, Kunming 650011, P.R.China*

⁵*National Astronomical Observatories, Chinese Academy of Sciences, Beijing 100012, P.R.China*

⁶*Université de Toulouse, UPS-OMP, IRAP, Toulouse, France*

⁷*CNRS, IRAP, 14 avenue Edouard Belin, 31400 Toulouse, France*

ABSTRACT

We analyze the photometric data and spectroscopic data that collect on the δ Scuti star AE UMa. The fundamental and the first overtone frequencies are confirmed as $f_0 = 11.62560 \text{ c d}^{-1}$ and $f_1 = 15.03124 \text{ c d}^{-1}$, respectively, from the frequency content by analyzing of the 40 nights light curve spanning from 2009 to 2012. Additionally, another 37 frequencies are identified as either the harmonics or the linear combinations of the fundamental and the first overtone frequencies, among which 25 are newly detected. The rate of period change of the fundamental mode is determined as $(1/P_0)(dP_0/dt) = 5.4(\pm 1.9) \times 10^{-9} \text{ yr}^{-1}$ as revealed from the $O - C$ diagram based on the 84 newly determined times of maximum light combined with those derived from the literature. The spectroscopic data suggests that AE UMa is a population I δ Scuti star. With these physical properties, we perform theoretical explorations based on the stellar evolution code MESA on this target, considering that the variation of pulsation period is caused by secular evolutionary effects. We finally constraint the AE UMa with the physical parameters as: the mass of $1.805 \pm 0.055 M_\odot$, the radius of $1.647 \pm 0.032 \times 10^{11} \text{ cm}$, the luminosity of $1.381 \pm 0.048 (\log L/L_\odot)$ and the age of $1.055 \pm 0.095 \times 10^9 \text{ yr}$. AE UMa can be the (Pop. I) δ Scuti star that locates just after the second turn-off of its evolutionary track leaving the main sequence, a star in the phase of the Hertzsprung Gap with a helium core and a hydrogen-burning shell.

Subject headings: stars: variables: δ Scuti – stars: oscillations – stars: individual: AE UMa – techniques: photometric – techniques: spectroscopic

1. INTRODUCTION

δ Scuti stars are a class of pulsating variable stars that lie in the classical instability strip crossing the main sequence on the Hertzsprung-Russell diagram. Their pulsations are driven by the κ -mechanism which drives both the Cepheids and the RR Lyrae stars as well. The amplitudes of pulsations in δ Scuti stars are from mmag up to tenths of a magnitude, periods between 0.03 and 0.3 days (see, e.g., Niu et al. 2013; Zong et al. 2015). These stars are found with masses between 1.5 and 2.5 M_{\odot} , luminosities between 10 and 50 L_{\odot} . The general consensus show that most (possibly all) δ Scuti stars are normal stars which evolve in the main-sequence or the immediate post-main-sequence stages, according to standard stellar-evolution theory (see, e.g., Baglin et al. 1973; Breger 1979, 1980). Nevertheless, observational proof of the validity of this hypothesis has not been found yet (Petersen & Christensen-Dalsgaard 1996).

The high-amplitude δ Scuti stars (hereafter HADS) are traditionally found with slow rotation, one or two dominant radial modes with amplitudes larger than 0.1 mag, although some of them may have low-amplitude nonradial modes (e.g., Poretti 2003). SX Phoenicis (SX Phe) stars is a subgroup of HADS with low metallicity and large spatial motion (see e.g., Fu et al. 2008a). They are old Pop. II stars and found to be members of globular clusters (Rodríguez & López-González 2000). However, some of them have been discovered in the general star fields (Rodríguez & Breger 2001). Interestingly, pulsations in the majority of the field SX Phe variables display simple frequency spectra with short periods ($\leq 0^{\text{d}}.08$) and large visual peak-to-peak amplitudes ($\geq 0^{\text{m}}.1$, e.g., Fu et al. 2008b). The period changes of pulsations can be determined based over long-term and high-precision photometric observations on such stars, which can constraint the stellar evolutionary phase of the star (e.g., Yang et al. 2012).

The star AE Ursae Majoris (hereafter AE UMa = HIP 47181, $\alpha_{2000} = 09^{\text{h}}36^{\text{m}}53^{\text{s}}$, $\delta_{2000} = 44^{\circ}04'01''$, $\langle V \rangle = 11^{\text{m}}.27$, $P_0 = 0^{\text{d}}.0860$, $\Delta V = 0^{\text{m}}.10$), was discovered to be a variable star by Geyer et al. (1955). The spectral type of AE UMa was classified in accordance with the type of variability by Götz & Wenzel (1961) as A9. The period of light variations was determined by Tsesevich (1973) and they classified it as a dwarf Cepheid. The beat phenomenon of the pulsations of this star was found by Szeidl (1974). AE UMa was listed as an SX Phe star by Garcia et al. (1995). However, Hintz et al. (1997a) showed strong evidence against this classification and reclassified it as a normal Population I, high-amplitude δ Scuti star. According to the measurement of Breger & Pamyatnykh (1998), AE UMa had fast period decreasing rate of $4.8 \times 10^{-7} \text{ yr}^{-1}$ hence it should be a pre-MS star. However, there is no other evidence for this star to be a pre-MS star. Recently, both Pócs & Szeidl (2001) and Zhou (2001) analyzed pulsations of the star with high-precision and longer photometric data. Their results are consistent with the classification with the

¹E-mail: jnfu@bnu.edu.cn

outcomes of Hintz et al. (1997a): AE UMa is a Pop. I, post-MS δ Scuti star, but with a stable fundamental frequency and the first overtone decreasing with a rate of $\sim 10^{-8}$ yr $^{-1}$.

In this paper, we present a detailed study of the pulsations and the period changes of AE UMa, mainly based on both photometric observations and spectroscopic observations. Based on the observational results, we perform theoretical explorations using the stellar code MESA and constraint the physical parameters on this star. The organization of the paper is: Section 2 describes photometry and data reduction, as well as spectral results; we present the pulsation analysis of the new data in Section 3; in Section 4, the rate of period change of the fundamental pulsations is determined before we conduct calculations of the stellar models with the constraints of the stellar parameters, the frequencies and their variations in Section 5; The conclusions of the study is given in the final section.

2. OBSERVATIONS AND DATA REDUCTION

Photometric observations for AE UMa were made with the 85-cm telescope located at the Xinglong Station of NAOC between March 2009 and May 2012. The 85-cm telescope was equipped with a standard Johnson-Cousin-Bessel multicolour filter system and a PI1024 BFT CCD camera mounted on the primary focus (Zhou et al. 2009). The CCD had 1024×1024 pixels, corresponding to a field of view of $16.5' \times 16.5'$. Since March 2012, the CCD camera has been replaced by a PI512 BFT with larger size of pixels, which has 512×512 pixels corresponding to a field of view of $15' \times 15'$. The observations were made through a standard Johnson V filter with the exposure time ranging from 15 to 120 seconds, depending on the atmospheric conditions. A journal of the new observations is listed in Table 1.

In total, 17277 CCD frames were collected for AE UMa during 40 nights. Figure 1 shows an image of AE UMa taken with the 85-cm telescope, where the comparison star (TYC 2998-1249-1) and the check star (TYC 2998-1166-1) are marked as well. The details of the three stars from SIMBAD (Wenger et al. 2000) are listed in Table 2.

The preliminary processing of the CCD frames (bias, dark subtraction and flat field correction) was performed with the standard routines of CCDPROC from the IRAF software. After that, we employed the IRAF DAOPHOT package to perform aperture photometry. In order to optimize the size of the aperture, we used 12 different size of apertures for the data in each night and adopted the aperture which brought the minimum variance of the magnitude differences between the check star and the comparison star. The data reduction was carried out with the standard process of aperture photometry.

The light curves were then produced by computing the magnitude differences between AE UMa and the comparison star. The standard deviations of the magnitude differences between the check star and the comparison star yielded an estimation of photometry precisions, with the typical

Table 1: Journal of photometric observations in V for AE UMa with the 85-cm telescope.

CCD	Year	Month	Nights	Frames
PI BFT1024	2009	Mar	5	4055
	2009	May	3	516
	2010	Feb	2	1385
	2011	Jan	5	1275
	2011	Feb	8	4759
	2012	Jan	1	328
	2012	Feb	6	1887
PI BFT512	2012	Mar	5	2516
	2012	Apr	5	556

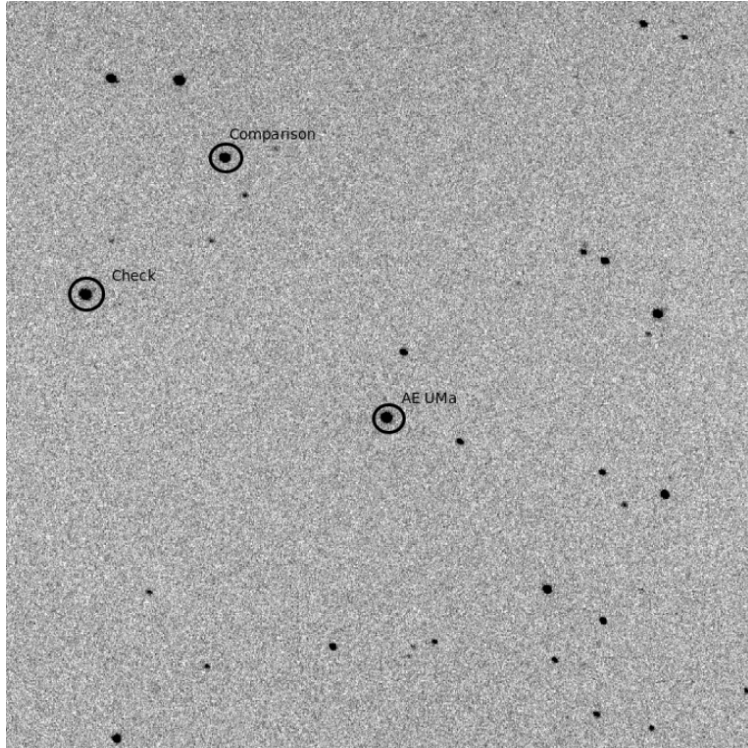


Fig. 1.— A CCD image ($16.5' \times 16.5'$) of AE UMa ($\alpha_{2000} = 09^{\text{h}}36^{\text{m}}53^{\text{s}}$, $\delta_{2000} = +44^{\circ}04'00''$) taken with the 85-cm telescope at the Xinglong Station. North is down and East is to the right. AE UMa, the comparison and the check star are marked.

value of $0^{\text{m}}.003$ in good observation conditions and $0^{\text{m}}.011$ in poor cases from night to night. As there were slight zero-point shifts, we adjusted it with the fitted light curves for every month by assuming that the pulsations were stable in one month.

Figure 2 shows the light curves of AE UMa in Johnson V band observed with the 85-cm telescope in 2009, 2010, 2011 and 2012, which was used to make pulsation analysis, and determination of new times of maximum light.

Spectroscopic observation for AE UMa was made with the 2.16 m telescope which locates at Xinglong station of NAOC on May 21, 2016. The BFOSC low-dispersion spectrometer was employed from the observations. The used grating was G7 with a slit width of $1.8''$ and a line dispersion of $95 \text{ \AA}/\text{mm}$. The center wavelength was at 530 nm with the wavelength range of 380-680 nm.

The data were reduced with IRAF and the obtained low-resolution spectrum is shown in Figure 3. With the results from spectroscopic observation, we used the automated 1D parametrization pipeline LASP which base on the stellar spectral template library (Wu et al. 2011) to get the stellar atmospheric parameters (see Table 3).

We note that the T_{eff} and $\log g$ correspond to a fixed phase since we only had acquired one spectrum. These values may vary differently from phase to phase during the pulsations of AE UMa. However, the metal to hydrogen ratio $[Fe/H]$ is not sensitive to the pulsations. The value of $[Fe/H]$ is $-0.32(\pm 0.23)$ which indicate that AE UMa is possibly a Pop. I δ Scuti star. This is consistent with the classification of the results obtained from Hintz et al. (1997a), Pócs & Szeidl (2001) and Zhou (2001) without spectroscopic data. Hence, AE UMa can be modeled as a single star in Section 5.

3. PULSATION ANALYSIS

Pulsation analysis was performed with the light curves of AE UMa in the years 2009, 2010, 2011 and 2012, respectively with the software PERIOD04 (Lenz & Breger 2005), which provides Fourier transformations of the light curves to search for significant peaks in the amplitude spectra until 150 c d^{-1} , since there is no significant ones above this frequency limit. Then, the light curves are fitted with the following formula,

$$m = m_0 + \Sigma A_i \sin(2\pi(f_i t + \phi_i)). \quad (1)$$

Table 2: The comparison star and the check star used in the photometry of AE UMa

Star name	$\alpha(2000)$	$\delta(2000)$	V	B	$B - V$
Object = AE Ursae Majoris	$09^{\text{h}}36^{\text{m}}53^{\text{s}}.155$	$+44^{\circ}04'00''.39$	11.35 ± 0.08	11.54 ± 0.06	0.19 ± 0.14
Comparison = TYC 2998-1249-1	$09^{\text{h}}37^{\text{m}}28^{\text{s}}.5826$	$+44^{\circ}01'16''.854$	11.32 ± 0.08	11.82 ± 0.08	0.50 ± 0.16
Check = TYC 2998-1166-1	$09^{\text{h}}37^{\text{m}}12^{\text{s}}.058$	$+43^{\circ}58'20''.12$	12.21 ± 0.18	13.10 ± 0.30	0.89 ± 0.48

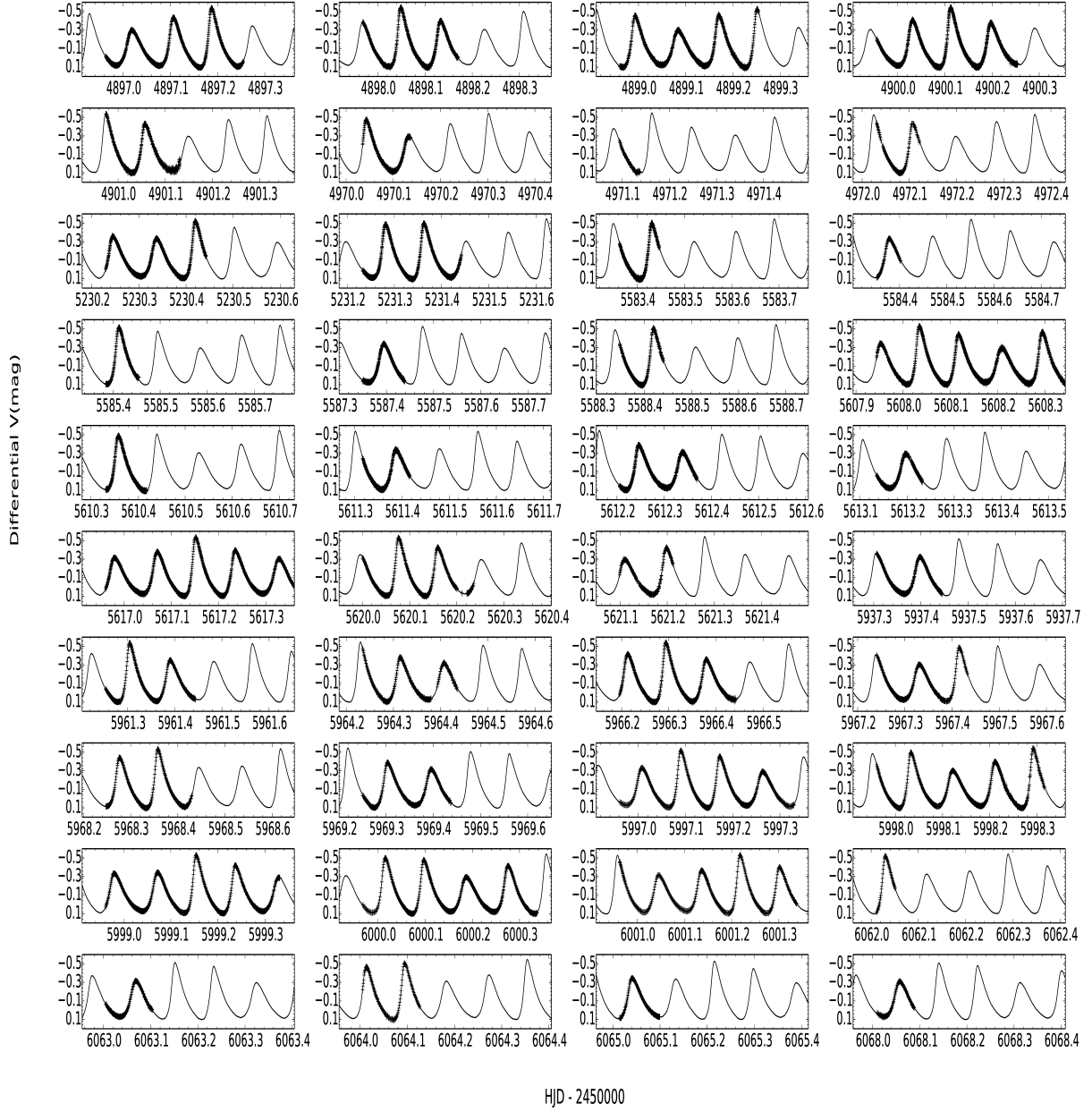


Fig. 2.— Light curves of AE UMA relative to the comparison star in the V band from 2009 to 2012, observed with the 85-cm telescope. The solid curves represent the fitting with a solution up to 18 frequencies listed in Table 3.

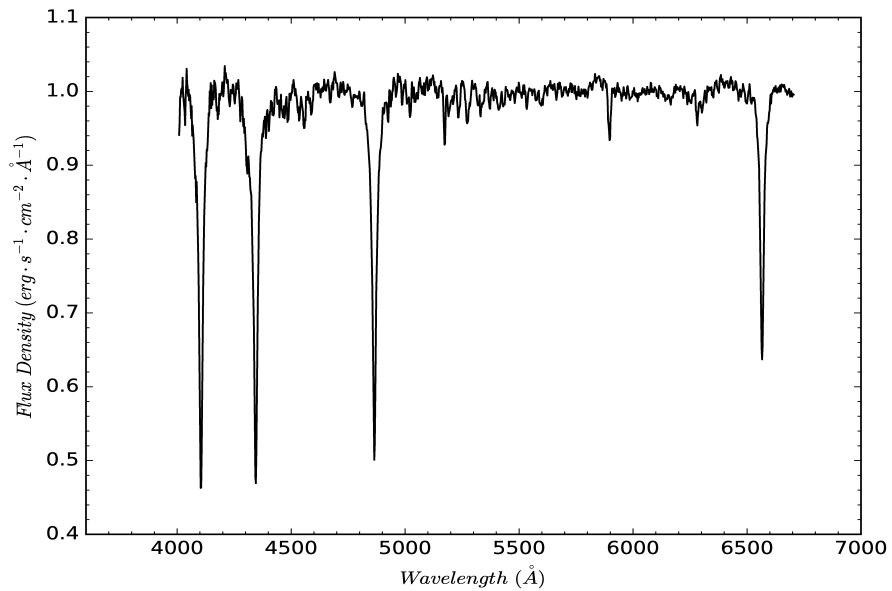


Fig. 3.— Spectroscopic observations results of AE UMa.

Table 3: Parameters of AE UMa derived from spectroscopic observations.

Parameters	Values	σ
T_{eff} (K)	7600	180
$\log g$	4.1	0.2
$[Fe/H]$	-0.32	0.23
RV (km/s)	150	27

Table 4 lists the solutions of 37 frequencies whose signal-to-noise ratios (S/N) are higher than 4.0 (Breger et al. 1993) and the averaged noise level is calculated over the whole frequency range, 0-150 c d^{-1} (e.g., Kepler et al. 2005). The solid curves in Figure 2 show the fits with the frequency solutions in different years. From Table 4, one notes that the 37 frequencies are composed of the fundamental and the first overtone frequencies, their harmonics and linear combinations. As can be noticed, no significant signals are detected in addition to these frequencies.

Figure 4 and Figure 5 show the window function and the amplitude spectra of the frequency pre-whitening process for the light curves in V in 2009, respectively.

As can be seen from Figure 2, the constructed curves fit well the light curves observed in 2009, 2010, 2011 and 2012, respectively, which shows that the fundamental and the first overtone frequencies, together with their harmonics and linear combinations, can explain the pulsation behavior of AE UMa.

To show the variations of the frequencies and amplitudes of pulsations of the star, we compare our results with those from Zhou (2001), which analysed the data for AE UMa from 1974 to 2001. By dividing the data into four segments of datasets following Zhou (2001), we resolved the pulsation parameters of the fundamental and the first overtone frequencies of AE UMa and listed them in Table 5.

4. The $O - C$ Diagram

With the new observations from 2009 to 2012, the light curves around the light maxima were fitted with a fourth polynomial by the nonlinear least-square method. The errors in polynomial fitting are consistent with the uncertainties estimated from Monte Carlo simulations of 100 iterations for each maximum. We obtained 84 times of maximum light in V band as listed in Table 6.

In order to make $O - C$ analysis for the period change of AE UMa, we combined the new times of maximum light with those provided from previous literatures ². We finally obtained 461 times of maximum light which are listed in Table 7. We discarded 17 times of maximum light, that were collected with either photograph (pg) or visual (vis), with large uncertainties, comparing to those collected with CCD or photoelectric photometer (pe). We finally used 444 data points to construct the $O - C$ (the Observed minus Calculated values) diagram. The used linear ephemeris formula is,

$$HJD_{\max} = 2442062.5824 + 0^{\text{d}}.08601707E \quad (2)$$

following Pócs & Szeidl (2001).

²Agerer et al. (1999a), Pócs & Szeidl (2001), Pejcha et al. (2001), Zhou (2001), Agerer & Hubscher (2003), Hubscher (2005), Hubscher et al. (2005), Klingenberg et al. (2006), Hubscher et al. (2006), Hubscher & Walter (2007), Samolyk (2010), Hubscher (2007), Hubscher et al. (2009), Hubscher et al. (2010) and Huebscher & Monninger (2011)

Table 4: Multi-frequency Solutions of the Light Curves of AE UMa in V Band in 2009, 2010, 2011 and 2012. Fre: Frequency in $c d^{-1}$. Amp: Amplitude in $mmag$. S/N: signal to noise ratio.

NO.	Marks	2009			2010			2011			2012		
		Fre	Amp	S/N	Fre	Amp	S/N	Fre	Amp	S/N	Fre	Amp	S/N
1	f_0	11.62525	220.45	1078.98	11.62944	216.36	2343.67	11.62549	218.93	1360.27	11.62558	218.26	1652.90
2	$2f_0$	23.25014	74.36	373.67	23.25888	73.25	727.33	23.25036	73.77	467.10	23.25108	73.57	565.07
3	f_1	15.03109	45.29	223.73	15.01105	43.95	464.85	15.03201	45.00	278.92	15.03117	45.11	343.71
4	$3f_0$	34.87873	28.48	147.81	34.88832	29.66	299.18	34.87620	27.70	175.13	34.87680	27.99	216.03
5	$f_0 + f_1$	26.65847	29.39	148.03	26.64049	28.76	294.84	26.65620	29.27	184.42	26.65665	29.72	228.20
6	$f_1 - f_0$	3.40580	25.47	123.84	3.42285	27.36	282.12	3.40660	24.36	153.48	3.40572	25.44	192.97
7	$2f_0 + f_1$	38.28217	16.24	84.60	39.34215	15.07	150.52	38.28280	16.11	101.50	38.28216	15.97	123.94
8	$4f_0$	46.51274	12.80	67.53	46.55900	13.02	126.33	46.50160	12.91	82.28	46.50233	12.99	100.78
9	$3f_0 + f_1$	49.90705	9.31	49.30	49.94062	10.26	97.83	49.90820	9.14	57.64	49.90796	9.11	71.07
10	$5f_0$	58.13493	6.23	33.19	57.15747	4.19	37.35	58.12700	5.89	36.99	58.12768	5.99	47.29
11	$2f_0 - f_1$	8.22789	6.16	29.75	9.15509	6.12	66.30	8.22257	6.44	40.27	8.21896	6.21	46.75
12	$4f_0 + f_1$	61.54123	4.99	26.63	60.33288	5.85	50.38	61.53360	5.15	31.85	61.53427	4.92	38.89
13	$f_0 + 2f_1$	41.70315	4.33	22.78	41.77526	3.15	31.22	41.68940	4.16	26.42	41.68853	4.22	32.67
14	$2f_1$	30.08096	3.77	19.17	30.06334	5.03	50.90	30.06400	3.32	20.86	30.06174	4.00	30.82
15	$6f_0$	69.76912	3.68	19.56	69.85913	3.51	28.13	69.75240	3.74	23.61	69.75322	3.29	26.59
16	$2f_1 - f_0$	19.81409	3.45	17.17	18.22771	3.46	36.34	19.84420	3.04	19.00	19.84574	3.16	24.26
17	$5f_0 + f_1$	73.16342	3.27	17.40	74.23048	3.31	25.21	73.15900	3.31	20.83	73.15980	3.42	27.88
18	$6f_0 + f_1$	84.76312	2.15	11.31	84.77368	2.83	19.70	84.78267	2.21	14.30	84.78566	2.19	18.38
19	$2f_0 + 2f_1$	53.34933	2.07	11.00	53.69338	1.82	16.55	53.31480	1.66	10.51	53.31282	2.26	17.81
20	$7f_0$	81.39280	2.00	10.53	80.56729	1.80	12.95	81.37984	1.90	12.21	81.38032	1.93	15.96
21	$7f_0 + f_1$	96.39730	1.45	7.94	96.36188	1.51	9.96	96.40807	1.60	10.48	96.41120	1.62	14.13
22	$3f_0 + 2f_1$	64.93553	1.60	8.59	63.83821	3.22	26.65	64.94397	1.64	10.21	64.93835	1.59	12.67
23	$4f_0 - f_1$	31.44828	1.76	9.02	31.54795	1.18	11.96	32.24212	1.34	8.43	31.47003	1.56	12.05
24	$2f_1 - 2f_0$	6.77661	1.41	6.81	7.79420	3.97	42.67	6.02561	2.05	12.85	7.78861	1.07	8.06
25	$2f_1 - f_0$	18.45877	1.40	6.98	18.22771	3.46	36.34	18.44237	2.04	12.70	18.43745	1.93	14.83
26	$4f_0 + 2f_1$	76.54723	1.32	7.07	—	—	—	75.79889	1.16	7.32	76.56296	1.18	9.64
27	$8f_0 + f_1$	108.00750	1.06	5.94	109.10478	1.26	7.68	108.03347	1.25	8.15	108.03549	0.99	8.77
28	$8f_0$	93.03898	1.22	6.65	—	—	—	93.01278	0.88	5.75	93.00586	1.18	10.13
29	$5f_0 + 2f_1$	88.20540	1.05	5.55	—	—	—	88.18550	1.06	6.91	88.18975	1.05	8.95
30	$6f_0 - f_1$	54.69265	1.20	6.36	—	—	—	53.31480	1.66	10.51	54.72485	0.98	7.74
31	$3f_1$	44.05397	1.03	5.45	—	—	—	43.09877	1.13	7.24	43.09681	1.00	7.75
32	$10f_0 + f_1$	131.28786	0.91	5.43	—	—	—	—	—	—	—	—	—
33	$9f_0 + f_1$	119.62969	0.82	4.78	118.71350	0.97	5.63	119.65510	0.72	4.76	118.65564	0.57	4.97
34	$6f_0 + 2f_1$	100.82309	0.78	4.35	100.77447	0.99	6.34	99.81467	1.01	6.64	99.81528	0.77	6.75
35	$7f_0 + 2f_1$	110.50225	0.73	4.16	110.99541	0.78	7.68	111.43957	0.69	5.19	—	—	—
36	$9f_0$	103.66567	0.71	4.01	104.89839	0.90	5.74	104.86428	0.69	4.48	103.65346	0.67	5.94
37	$8f_0 + 2f_1$	—	—	—	—	—	—	—	—	—	123.06760	0.54	4.82

Table 5: Frequencies and amplitudes of AE UMa for different segments of observations, including the data sets of Zhou (2001) and our data. (The data of 1981-1987 has not been used due to its large scatters.)

Years	f_0	f_1	A_0	A_1
1974-1977	11.62557	15.03097	216.9	34.1
*1981-1987	11.62290	15.07259	219.6	29.4
1996-1998	11.62560	15.03122	210.9	36.8
2000-2001	11.62561	15.03119	207.0	38.6
2009-2012	11.62560	15.03123	219.0	45.1
Mean	11.62560	15.03120	213.5	38.7
σ	0.000015	0.000123	5.5	4.7

Table 6: Newly Determined Times of Maximum Light of AE UMa. T_{max} is in $HJD - 2450000$. σ is the estimated uncertainty of the times of maximum light in days.

T_{max}	σ	T_{max}	σ
4897.01876	0.00009	5621.11032	0.00017
4897.10688	0.00008	5621.19860	0.00019
4897.18828	0.00004	5937.39814	0.00012
4898.04897	0.00010	5961.30507	0.00004
4898.13312	0.00015	5961.39070	0.00010
4898.99305	0.00013	5964.31479	0.00014
4899.08369	0.00023	5964.40728	0.00019
4899.17058	0.00013	5966.21331	0.00007
4900.03182	0.00010	5966.29416	0.00005
4900.11285	0.00008	5966.37965	0.00008
4900.19779	0.00014	5967.33106	0.00009
4901.05755	0.00027	5967.41592	0.00007
4970.04314	0.00008	5968.27734	0.00007
4972.10776	0.00024	5968.35817	0.00004
5230.24553	0.00009	5969.30381	0.00007
5230.33788	0.00010	5969.39594	0.00014
5230.42007	0.00008	5997.00800	0.00008
5231.28178	0.00008	5997.09064	0.00004
5231.36352	0.00006	5997.17295	0.00004
5583.43132	0.00012	5997.26391	0.00010
5584.37869	0.00018	5998.03373	0.00008
5585.41321	0.00008	5998.12209	0.00014
5587.39457	0.00009	5998.21192	0.00008
5588.42008	0.00008	5998.29274	0.00006
5607.95282	0.00018	5998.98078	0.00009
5608.03484	0.00011	5999.07267	0.00009
5608.11800	0.00011	5999.15466	0.00005
5608.20986	0.00022	5999.23746	0.00005
5608.29535	0.00012	6000.01612	0.00005
5608.37632	0.00011	6000.09780	0.00004
5610.35912	0.00010	6000.18742	0.00009
5611.38774	0.00016	6000.27618	0.00006
5612.24692	0.00014	6001.04594	0.00006
5612.33917	0.00022	6001.13682	0.00006
5613.19799	0.00021	6001.21857	0.00003
5616.98003	0.00011	6001.30228	0.00006
5617.07053	0.00008	6062.03120	0.00005
5617.15198	0.00005	6063.06910	0.00015
5617.23583	0.00006	6064.01367	0.00008
5617.32810	0.00010	6064.09479	0.00008
5620.07717	0.00010	6065.04189	0.00009
5620.16024	0.00017	6068.05799	0.00021

A linear fit to the 444 times of light maxima yields the ephemeris formula,

$$\begin{aligned} HJD_{\max} &= 2442062.5818(\pm 0.0002) \\ &+ 0^{\text{d}}.086017078(\pm 0.000000002)E \end{aligned} \tag{3}$$

with a standard deviation of $\sigma_0 = 0.00246$ days. The $O - C$ values are listed in Table 7 as well. The $O - C$ diagram is shown in Figure 6.

Table 7. Times of Maximum Light and $O - C$ values of AE UMa. T_{max} is the observed times of maximum light in $HJD - 2400000$. E : Cycle number. $O - C$ is in days. Det: detector (pg=photograph, vis=visual, pe=photoelectric photometer). Points not used in the $O - C$ analysis are marked with asterisk.

NO.	T_{max}	E	$O - C$	Det	S	NO.	T_{max}	E	$O - C$	Det	S
1	28632.398	-156133	—	pg	(1)*	26	42087.5263	290	-0.000808	pe	(4)
2	31875.122	-118434	—	pg	(2)*	27	42087.6155	291	0.002375	pe	(4)
3	33379.256	-100948	—	pg	(2)*	28	42095.5298	383	0.003105	pe	(3)
4	35601.188	-75117	—	pg	(2)*	29	42095.6123	384	-0.000412	pe	(3)
5	35604.337	-75080	—	vis	(1)*	30	42103.3513	474	-0.002947	pe	(4)
6	35607.173	-75047	—	pg	(2)*	31	42106.4523	510	0.001439	pe	(3)
7	35981.202	-70699	—	pg	(2)*	32	42119.5252	662	-0.000255	pe	(3)
8	38106.402	-45992	—	vis	(1)*	33	42121.5025	685	-0.001347	pe	(3)
9	41059.368	-11662	—	vis	(1)*	34	42122.3628	695	-0.001218	pe	(4)
10	41773.223	-3363	—	vis	(1)*	35	42122.4484	696	-0.001635	pe	(4)
11	42062.5832	0	0.001039	pe	(3)	36	42128.2968	764	-0.002395	pe	(3)
12	42065.5959	35	0.003142	pe	(4)	37	42128.3872	765	0.001988	pe	(3)
13	42065.6778	36	-0.000975	pe	(4)	38	42128.4727	766	0.001471	pe	(3)
14	42068.3432	67	-0.002104	pe	(4)	39	42128.5557	767	-0.001546	pe	(3)
15	42068.4302	68	-0.001121	pe	(4)	40	42133.4627	824	0.002482	pe	(3)
16	42068.5203	69	0.002962	pe	(4)	41	42133.5442	825	-0.002035	pe	(3)
17	42068.6029	70	-0.000455	pe	(4)	42	42134.4055	835	-0.000906	pe	(3)
18	42068.6871	71	-0.002272	pe	(4)	43	42147.3933	986	-0.001682	pe	(3)
19	42069.3808	79	0.003292	pe	(4)	44	42148.4295	998	0.002313	pe	(3)
20	42069.4651	80	0.001574	pe	(4)	45	42148.5117	999	-0.001504	pe	(3)
21	42069.5473	81	-0.002243	pe	(4)	46	42159.4365	1126	-0.000871	pe	(3)
22	42069.6363	82	0.000740	pe	(4)	47	42161.4145	1149	-0.001263	pe	(3)
23	42086.4965	278	0.001597	pe	(4)	48	42453.5306	4545	0.000899	pe	(3)
24	42086.5787	279	-0.002221	pe	(4)	49	42453.6137	4546	-0.002018	pe	(3)
25	42087.4390	289	-0.002091	pe	(4)	50	42460.4989	4626	0.001817	pe	(3)
51	42532.407	5462	—	vis	(5)*	76	46468.4601	51221	-0.002180	pe	(3)
52	42830.6280	8929	-0.000499	pe	(3)	77	46468.5468	51222	-0.001497	pe	(3)
53	42837.5120	9009	0.002136	pe	(3)	78	46855.6279	55722	0.002780	pe	(8)
54	42838.4591	9020	0.003049	pe	(3)	79	46856.5729	55733	0.001592	pe	(8)
55	42866.496	9346	—	vis	(5)*	80	46856.6561	55734	-0.001225	pe	(8)
56	42869.3377	9379	0.001523	pe	(3)	81	46857.6017	55745	-0.001812	pe	(8)
57	42869.4205	9380	-0.001694	pe	(3)	82	46857.6925	55746	0.002970	pe	(8)
58	43162.5708	12788	0.002457	pe	(3)	83	46858.6382	55757	0.002483	pe	(8)
59	44633.4626	29888	0.002451	pe	(3)	84	46859.6666	55769	-0.001322	pe	(8)
60	44633.5440	29889	-0.002166	pe	(3)	85	46878.4181	55987	-0.001544	pe	(8)
61	44633.6309	29890	-0.001283	pe	(3)	86	46878.5064	55988	0.000739	pe	(8)
62	44634.4046	29899	-0.001737	pe	(3)	87	46878.5946	55989	0.002922	pe	(8)
63	44634.4902	29900	-0.002154	pe	(3)	88	46884.5262	56058	-0.000656	pe	(8)
64	44634.5810	29901	0.002629	pe	(3)	89	46884.6117	56059	-0.001173	pe	(8)
65	44692.4709	30574	0.003043	pe	(3)	90	46886.5907	56082	-0.000566	pe	(8)
66	44696.343	30619	—	vis	(6)*	91	48683.317	76970	—	vis	(9)*

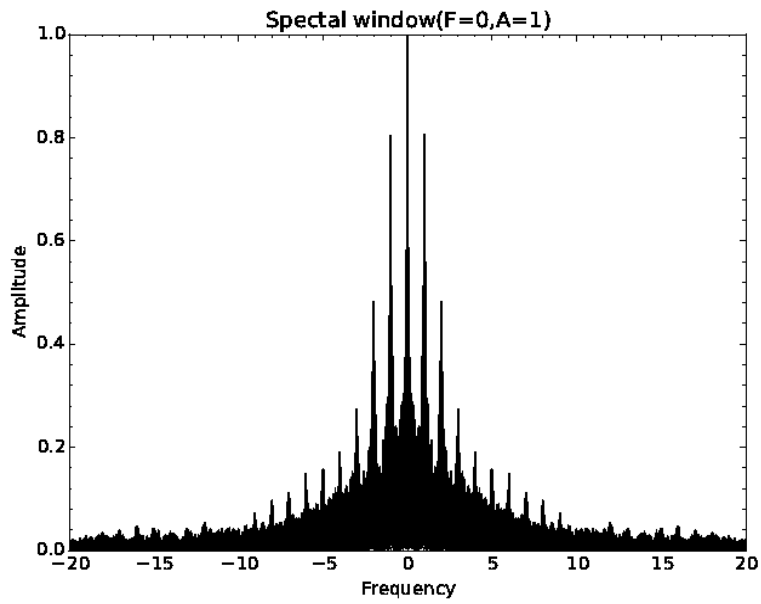


Fig. 4.— Spectral window of the light curves in V for AE UMa in 2009.

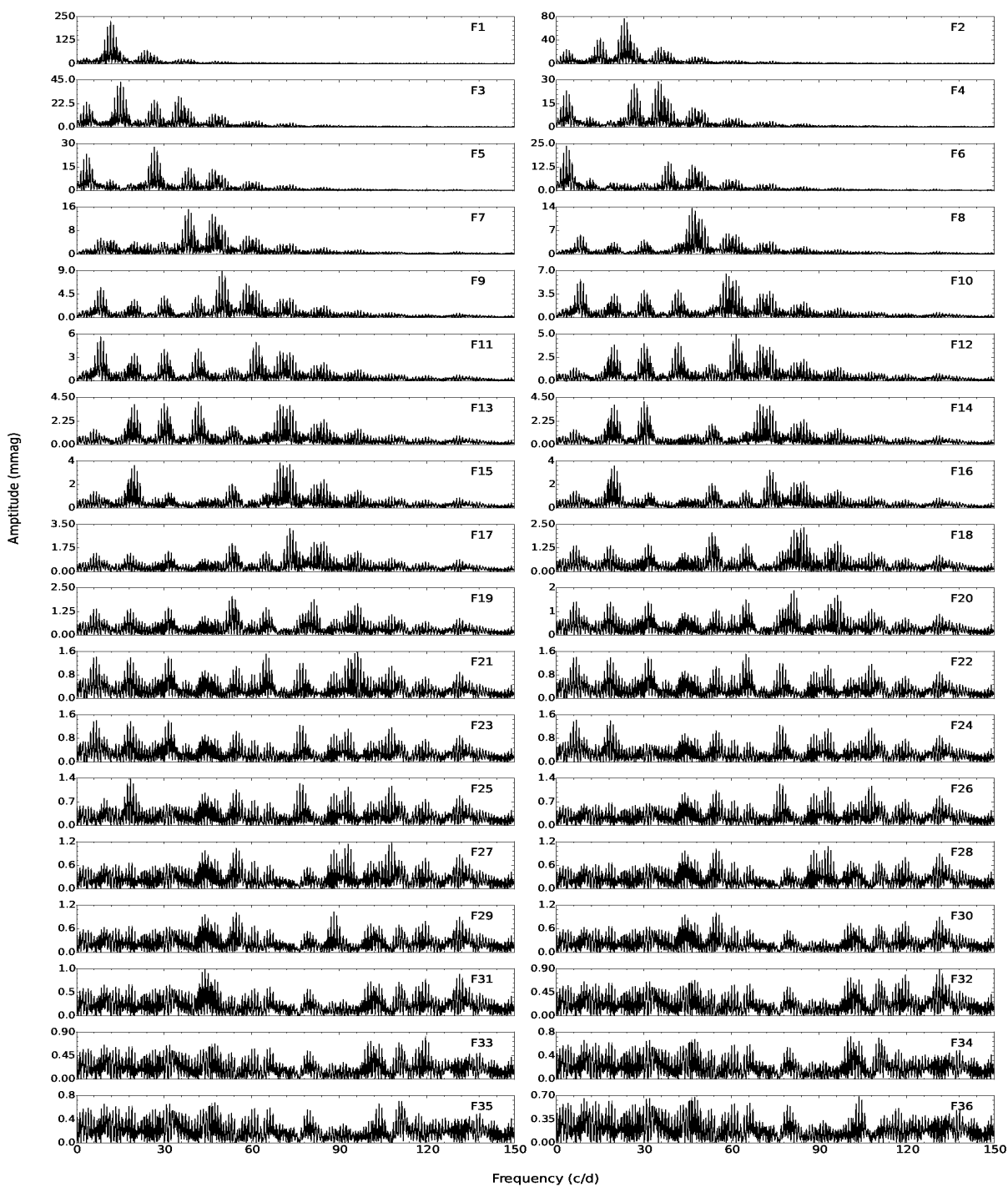


Fig. 5.— Amplitude spectrum of the light curves in V for AE UMa collected in 2009, and the amplitude spectra of the frequency pre-whitening process. Note that the y-axis scales are optimized concerning the highest peaks in the panels.

Table 7—Continued

NO.	T_{max}	E	$O - C$	Det	S	NO.	T_{max}	E	$O - C$	Det	S
67	44696.426	30620	—	vis	(6)*	92	50151.4564	94038	0.000981	pe	(3)
68	44696.520	30621	—	vis	(6)*	93	50151.5384	94039	-0.003036	pe	(3)
69	45355.4902	38282	0.002786	pe	(3)	94	50152.3170	94048	0.001411	pe	(3)
70	45355.5727	38283	-0.000731	pe	(3)	95	50152.4862	94050	-0.001424	pe	(3)
71	45382.3228	38594	-0.001939	pe	(3)	96	50152.5756	94051	0.001959	pe	(3)
72	45382.4104	38595	-0.000356	pe	(3)	97	50458.8815	97612	0.001034	CCD	(10)
73	45382.4997	38596	0.002927	pe	(3)	98	50458.9636	97613	-0.002883	CCD	(10)
74	45382.5807	38597	-0.002090	pe	(3)	99	50459.8240	97623	-0.002654	CCD	(10)
75	46114.332	47104	—	vis	(7)*	100	50459.9113	97624	-0.001371	CCD	(10)
101	50467.7388	97715	-0.001425	CCD	(10)	126	50902.2976	102768	-0.000923	pe	(3)
102	50467.8236	97716	-0.002642	CCD	(10)	127	50902.3819	102779	-0.002640	pe	(3)
103	50490.3607	97978	-0.002018	pe	(3)	128	50903.3321	102780	0.001372	pe	(3)
104	50505.6697	98156	-0.004058	CCD	(10)	129	50903.4192	102781	0.002455	pe	(3)
105	50505.7595	98157	-0.000275	CCD	(10)	130	50903.5009	107036	-0.001862	CCD	(13)
106	50505.8461	98158	0.000308	CCD	(10)	131	51269.5080	107198	0.002550	CCD	(13)
107	50516.7676	98285	-0.002362	CCD	(10)	132	51283.4410	107199	0.000782	CCD	(13)
108	50554.4432	98723	-0.002243	pe	(3)	133	51283.5250	107200	-0.001235	CCD	(13)
109	50813.3550	101733	-0.001860	pe	(3)	134	51283.6090	107604	-0.003252	CCD	(13)
110	50813.4408	101734	-0.002077	pe	(3)	135	51318.3630	107605	-0.000154	CCD	(13)
111	50813.6151	101736	0.000189	pe	(3)	136	51318.4460	110972	-0.003171	CCD	(14)
112	50813.6985	101737	-0.002428	pe	(3)	137	51608.0716	110973	0.002908	CCD	(14)
113	50848.4540	102141	0.002170	pe	(3)	138	51608.1577	110974	0.002991	CCD	(14)
114	50848.5391	102142	0.001253	pe	(3)	139	51608.2395	110975	-0.001226	CCD	(14)
115	50848.6212	102143	-0.002664	pe	(3)	140	51608.3264	110983	-0.000343	CCD	(14)
116	50849.4815	102153	-0.002535	pe	(3)	141	51609.0186	110984	0.003720	CCD	(14)
117	50849.5688	102154	-0.001252	pe	(3)	142	51609.1006	110985	-0.000297	CCD	(14)
118	50862.3840	102303	-0.002597	CCD	(13)	143	51609.1865	110986	-0.000414	CCD	(14)
119	50862.3840	102418	-0.002597	pe	(3)	144	51609.2770	110987	0.004069	CCD	(14)
120	50872.2809	102419	0.002339	pe	(3)	145	51609.3583	110995	-0.000648	CCD	(14)
121	50872.3634	102420	-0.001178	pe	(3)	146	51610.0450	111006	-0.002085	CCD	(14)
122	50872.4481	102421	-0.002496	pe	(3)	147	51610.9969	111007	0.003627	CCD	(14)
123	50872.5394	102733	0.002787	pe	(3)	148	51611.0821	111008	0.002810	CCD	(14)
124	50899.3729	102734	-0.001042	pe	(3)	149	51611.1627	111018	-0.002607	CCD	(14)
125	50899.4570	102767	-0.002959	pe	(3)	150	51612.0246	111019	-0.000878	CCD	(14)
151	51612.1090	111020	-0.002495	CCD	(14)	176	51941.2979	114847	-0.000978	CCD	(14)
152	51612.2010	111021	0.003488	CCD	(14)	177	51941.3881	114856	0.003205	CCD	(14)
153	51612.2846	111022	0.001071	CCD	(14)	178	51942.1562	114857	-0.002849	CCD	(14)
154	51612.3704	111029	0.000854	CCD	(14)	179	51942.2473	114858	0.002234	CCD	(14)
155	51612.9692	111030	-0.002466	CCD	(14)	180	51942.3311	114859	0.000017	CCD	(14)
156	51613.0609	111031	0.003217	CCD	(14)	181	51942.4141	119265	-0.003000	CCD	(15)
157	51613.1453	111032	0.001600	CCD	(14)	182	52321.4089	119846	0.000521	CCD	(15)

Table 7—Continued

NO.	T_{max}	E	$O - C$	Det	S	NO.	T_{max}	E	$O - C$	Det	S
158	51613.2276	111033	-0.002117	CCD	(14)	183	52371.3836	123496	-0.000706	CCD	(15)
159	51613.3156	111053	-0.000134	CCD	(14)	184	52685.3460	123497	-0.000673	CCD	(15)
160	51615.0341	111054	-0.001976	CCD	(14)	185	52685.4369	124020	0.004210	CCD	(15)
161	51615.1260	111055	0.003907	CCD	(14)	186	52730.4187	124124	-0.000926	CCD	(15)
162	51615.2098	111056	0.001690	CCD	(14)	187	52739.3617	124195	-0.003703	CCD	(16)
163	51615.2919	111064	-0.002227	CCD	(14)	188	52745.4702	126928	-0.002416	CCD	(17)
164	51615.9855	111065	0.003236	CCD	(14)	189	52980.5608	126929	0.003484	CCD	(17)
165	51616.0705	111066	0.002219	CCD	(14)	190	52980.6421	126930	-0.001233	CCD	(17)
166	51616.1526	111067	-0.001698	CCD	(14)	191	52980.7279	127195	-0.001451	CCD	(16)
167	51616.2389	114706	-0.001415	CCD	(14)	192	53003.5231	127483	-0.000779	CCD	(16)
168	51929.2556	114707	-0.000886	CCD	(14)	193	53028.2942	127484	-0.002600	CCD	(16)
169	51929.3464	114717	0.003897	CCD	(14)	194	53028.3871	127485	0.004283	CCD	(16)
170	51930.2058	114718	0.003126	CCD	(14)	195	53028.4705	127486	0.001666	CCD	(16)
171	51930.2885	114719	-0.000191	CCD	(14)	196	53028.5522	127487	-0.002651	CCD	(16)
172	51930.3721	114729	-0.002608	CCD	(14)	197	53028.6420	127961	0.001132	CCD	(16)
173	51931.2315	114730	-0.003379	CCD	(14)	198	53069.4119	127962	-0.001068	CCD	(16)
174	51931.3203	114845	-0.000596	CCD	(14)	199	53069.5029	127973	0.003915	CCD	(16)
175	51941.2102	114846	-0.002661	CCD	(14)	200	53070.4493	127974	0.004127	CCD	(16)
201	53070.5320	128205	0.000810	CCD	(16)	226	54079.8580	139709	0.002285	CCD	(21)
202	53090.4053	128251	0.004162	CCD	(16)	227	54079.9437	139973	0.001967	CCD	(21)
203	53094.3575	128437	-0.000424	CCD	(19)	228	54102.6471	139974	-0.003144	CCD	(21)
204	53110.3619	131915	0.004798	CCD	(18)	229	54102.7365	139975	0.000238	CCD	(21)
205	53409.5286	131916	0.004064	CCD	(18)	230	54102.8254	139985	0.003121	CCD	(21)
206	53409.6108	131917	0.000247	CCD	(18)	231	54103.6849	139986	0.002450	CCD	(21)
207	53409.6940	132122	-0.002570	CCD	(19)	232	54103.7677	139997	-0.000767	CCD	(21)
208	53427.3272	132123	-0.002873	CCD	(19)	233	54104.7117	140031	-0.002955	CCD	(21)
209	53427.4181	132124	0.002010	CCD	(19)	234	54107.6358	140032	-0.003436	CCD	(21)
210	53427.5031	132402	0.000993	CCD	(17)	235	54107.7251	140033	-0.000153	CCD	(21)
211	53451.4136	132403	-0.001258	CCD	(17)	236	54107.8138	140034	0.002530	CCD	(21)
212	53451.5042	132785	0.003325	CCD	(17)	237	54107.8944	140067	-0.002887	CCD	(21)
213	53484.3616	136052	0.002197	CCD	(20)	238	54110.7388	140068	0.002949	CCD	(21)
214	53765.3803	136053	0.003066	CCD	(20)	239	54110.8207	140069	-0.001168	CCD	(21)
215	53765.4660	136054	0.002749	CCD	(20)	240	54110.9051	140070	-0.002785	CCD	(21)
216	53765.5462	136063	-0.003068	CCD	(20)	241	54110.9977	140241	0.003798	CCD	(21)
217	53766.3278	136064	0.004378	CCD	(20)	242	54125.7056	140242	0.002775	CCD	(21)
218	53766.4079	136065	-0.001539	CCD	(20)	243	54125.7883	140243	-0.000542	CCD	(21)
219	53766.4943	136066	-0.001156	CCD	(20)	244	54125.8716	140244	-0.003259	CCD	(21)
220	53766.5849	136389	0.003427	CCD	(18)	245	54125.9649	140309	0.004024	CCD	(21)
221	53794.3619	136400	-0.003093	CCD	(18)	246	54131.5550	140310	0.003013	CCD	(21)
222	53795.3115	136401	0.000319	CCD	(18)	247	54131.6392	140311	0.001196	CCD	(21)
223	53795.3998	136776	0.002602	CCD	(18)	248	54131.7212	140312	-0.002821	CCD	(21)

Table 7—Continued

NO.	T_{max}	E	$O - C$	Det	S	NO.	T_{max}	E	$O - C$	Det	S
224	53827.6570	139707	0.003393	CCD	(21)	249	54131.8106	140313	0.000562	CCD	(21)
225	54079.7666	139708	-0.003098	CCD	(21)	250	54131.8989	140367	0.002845	CCD	(21)
251	54136.5446	140368	0.003622	CCD	(21)	276	54198.3850	141086	-0.002266	CCD	(22)
252	54136.6275	140369	0.000505	CCD	(21)	277	54198.4741	141087	0.000817	CCD	(22)
253	54136.7104	140370	-0.002612	CCD	(21)	278	54202.4288	141133	-0.001270	CCD	(22)
254	54136.7998	140371	0.000771	CCD	(21)	279	54414.8939	143603	0.001615	CCD	(21)
255	54136.8882	140372	0.003154	CCD	(21)	280	54414.9804	143604	0.002098	CCD	(21)
256	54136.9697	140380	-0.001364	CCD	(21)	281	54417.7271	143636	-0.003749	CCD	(21)
257	54137.6581	140381	-0.001100	CCD	(21)	282	54417.9058	143638	0.002917	CCD	(21)
258	54137.7491	140382	0.003883	CCD	(21)	283	54417.9856	143639	-0.003300	CCD	(21)
259	54137.8311	140404	-0.000134	CCD	(21)	284	54440.6958	143903	-0.001612	CCD	(21)
260	54139.7226	140405	-0.001010	CCD	(21)	285	54442.7619	143927	0.000078	CCD	(21)
261	54139.8124	140406	0.002772	CCD	(21)	286	54442.8516	143928	0.003761	CCD	(21)
262	54139.8942	140428	-0.001445	CCD	(21)	287	54442.9342	143929	0.000344	CCD	(21)
263	54141.7876	140429	-0.000421	CCD	(21)	288	54451.6243	144030	0.002717	CCD	(21)
264	54141.8768	140430	0.002762	CCD	(21)	289	54460.6513	144135	-0.002077	CCD	(21)
265	54141.9575	140554	-0.002555	CCD	(21)	290	54460.7433	144136	0.003906	CCD	(21)
266	54152.6241	140565	-0.002074	CCD	(21)	291	54460.8247	144137	-0.000712	CCD	(21)
267	54153.5746	140578	0.002238	CCD	(21)	292	54460.9089	144138	-0.002529	CCD	(21)
268	54154.6883	140579	-0.002284	CCD	(21)	293	54467.7955	144218	0.002704	CCD	(21)
269	54154.7800	140580	0.003399	CCD	(21)	294	54468.7392	144229	0.000216	CCD	(21)
270	54154.8618	140773	-0.000818	CCD	(22)	295	54468.8220	144230	-0.003001	CCD	(21)
271	54171.4664	140808	0.002483	CCD	(22)	296	54468.9120	144231	0.000982	CCD	(21)
272	54175.4206	140819	-0.000103	CCD	(22)	297	54469.6815	144240	-0.003672	CCD	(21)
273	54196.4976	141064	0.002710	CCD	(22)	298	54469.7701	144241	-0.001089	CCD	(21)
274	54197.3590	141074	0.003939	CCD	(22)	299	54469.8603	144242	0.003094	CCD	(21)
275	54197.4402	141075	-0.000878	CCD	(22)	300	54469.9414	144243	-0.001823	CCD	(21)
301	54506.5887	144669	0.002196	CCD	(23)	326	54837.7565	148519	0.004191	CCD	(21)
302	54512.5199	144738	-0.001784	CCD	(23)	327	54843.6886	148588	0.001112	CCD	(21)
303	54513.4650	144749	-0.002872	CCD	(23)	328	54843.7704	148589	-0.003105	CCD	(21)
304	54513.5559	144750	0.002011	CCD	(23)	329	54843.8567	148590	-0.002822	CCD	(21)
305	54524.4815	144877	0.003441	CCD	(23)	330	54843.9494	148591	0.003861	CCD	(21)
306	54769.8859	147730	0.001077	CCD	(21)	331	54846.6137	148622	0.001631	CCD	(21)
307	54770.8336	147741	0.002589	CCD	(21)	332	54846.6960	148623	-0.002086	CCD	(21)
308	54770.9152	147742	-0.001828	CCD	(21)	333	54847.7336	148635	0.003309	CCD	(21)
309	54781.8384	147869	-0.002798	CCD	(21)	334	54847.8164	148636	0.000092	CCD	(21)
310	54781.9301	147870	0.002884	CCD	(21)	335	54847.8988	148637	-0.003525	CCD	(21)
311	54788.8080	147950	-0.000583	CCD	(21)	336	54855.6469	148727	0.003036	CCD	(21)
312	54788.8912	147951	-0.003400	CCD	(21)	337	54855.7316	148728	0.001719	CCD	(21)
313	54788.9833	147952	0.002683	CCD	(21)	338	54855.8119	148729	-0.003998	CCD	(21)
314	54791.7333	147984	0.000136	CCD	(21)	339	54855.9023	148730	0.000385	CCD	(21)

Table 7—Continued

NO.	T_{max}	E	$O - C$	Det	S	NO.	T_{max}	E	$O - C$	Det	S
315	54791.8157	147985	-0.003481	CCD	(21)	340	54864.5873	148831	-0.002341	CCD	(21)
316	54791.9080	147986	0.002802	CCD	(21)	341	54864.6724	148832	-0.003258	CCD	(21)
317	54791.9938	147987	0.002585	CCD	(21)	342	54864.7649	148833	0.003224	CCD	(21)
318	54807.8222	148171	0.003840	CCD	(21)	343	54864.8477	148834	0.000007	CCD	(21)
319	54807.9032	148172	-0.001177	CCD	(21)	344	54864.9296	148835	-0.004110	CCD	(21)
320	54807.9866	148173	-0.003795	CCD	(21)	345	54868.6346	148878	0.002155	CCD	(21)
321	54816.6793	148274	0.001179	CCD	(21)	346	54868.7166	148879	-0.001862	CCD	(21)
322	54816.7612	148275	-0.002938	CCD	(21)	347	54868.8033	148880	-0.001179	CCD	(21)
323	54816.8501	148276	-0.000055	CCD	(21)	348	54868.8941	148881	0.003604	CCD	(21)
324	54816.9399	148277	0.003728	CCD	(21)	349	54878.6935	148995	-0.002945	CCD	(21)
325	54837.6637	148518	-0.002591	CCD	(21)	350	54878.7811	148996	-0.001362	CCD	(21)
351	54878.8721	148997	0.003621	CCD	(21)	376	54924.3742	149526	0.003777	CCD	(24)
352	54894.4412	149178	0.003628	CCD	(24)	377	54970.0431	150057	0.000360	CCD	(26)
353	54894.5227	149179	-0.000890	CCD	(24)	378	54972.1078	150081	0.000715	CCD	(26)
354	54894.6071	149180	-0.002507	CCD	(24)	379	55230.2455	153082	0.002798	CCD	(26)
355	54897.0188	149208	0.000058	CCD	(26)	380	55230.3379	153083	-0.001819	CCD	(26)
356	54897.1069	149209	0.004345	CCD	(26)	381	55230.4201	153084	-0.001290	CCD	(26)
357	54897.1883	149210	-0.000972	CCD	(26)	382	55231.2818	153094	-0.003207	CCD	(26)
358	54898.0490	149220	-0.003829	CCD	(26)	383	55231.3635	153095	-0.003478	CCD	(26)
359	54898.1331	149221	0.004153	CCD	(26)	384	55259.4108	153421	0.001205	CCD	(25)
360	54898.3084	149223	-0.001064	CCD	(24)	385	55293.3826	153816	0.002087	CCD	(25)
361	54898.9930	149231	-0.003252	CCD	(26)	386	55293.4752	153817	0.003117	CCD	(25)
362	54899.0837	149232	0.003172	CCD	(26)	387	55302.3318	153920	-0.001901	CCD	(25)
363	54899.1706	149233	-0.000545	CCD	(26)	388	55303.3591	153932	-0.002918	CCD	(25)
364	54900.0318	149243	0.002679	CCD	(26)	389	55304.3959	153944	-0.003389	CCD	(25)
365	54900.1128	149244	0.002702	CCD	(26)	390	55304.4775	153945	-0.003497	CCD	(25)
366	54900.1978	149245	-0.002250	CCD	(26)	391	55305.3388	153955	-0.003207	CCD	(25)
367	54901.0575	149255	0.004333	CCD	(26)	392	55305.4238	153956	-0.002804	CCD	(25)
368	54904.4199	149294	0.001172	CCD	(24)	393	55309.3848	154002	0.003579	CCD	(25)
369	54904.5006	149295	-0.003733	CCD	(24)	394	55310.4124	154014	-0.000238	CCD	(25)
370	54909.3147	149351	0.000862	CCD	(24)	395	55311.3662	154025	0.001291	CCD	(25)
371	54909.4087	149352	-0.003555	CCD	(24)	396	55311.4488	154026	-0.003026	CCD	(25)
372	54909.4895	149353	-0.002426	CCD	(24)	397	55583.4313	157188	-0.003191	CCD	(26)
373	54910.4335	149364	-0.003443	CCD	(24)	398	55584.3787	157199	-0.001979	CCD	(26)
374	54912.3323	149386	0.000770	CCD	(24)	399	55585.4132	157211	0.000316	CCD	(26)
375	54912.4146	149387	-0.003835	CCD	(24)	400	55587.3946	157234	0.003323	CCD	(26)
401	55588.4201	157246	-0.003383	CCD	(26)	426	55964.4073	161617	0.003096	CCD	(26)
402	55607.9528	157473	0.003437	CCD	(26)	427	55966.2133	161638	0.002737	CCD	(26)
403	55608.0348	157474	-0.000580	CCD	(26)	428	55966.2942	161639	-0.002380	CCD	(26)
404	55608.1180	157475	-0.003397	CCD	(26)	429	55966.3797	161640	-0.002897	CCD	(26)
405	55608.2099	157476	0.002486	CCD	(26)	430	55967.3311	161651	0.002315	CCD	(26)

In addition, we made a quadratic fit with a second-order polynomial,

$$\begin{aligned}
 HJD_{max} &= 2442062.5822(\pm 0.0002) \\
 &+ 0.086017060(\pm 0.000000006)E \\
 &+ 0.5 \times 1.09(\pm 0.38) \times 10^{-13} E^2
 \end{aligned}
 \tag{4}$$

with the standard deviation of $\sigma_1 = 0.00244$ days. The quadratic terms differ from zero by a factor of 2.87σ with the significance of ~ 99.5 percent and the statistic test proposed by (Pringle 1975) suggests that the small improvement in period deviation gives the quadratic term in the fit with a significance of ~ 99.3 percent. From the values in equation (4), we take the period change rate of AE UMa as $(1/P_0)(dP_0/dt) = 5.4(\pm 1.9) \times 10^{-9} \text{ yr}^{-1}$ that is different from the result of $-0.35 \times 10^{-10} \text{ yr}^{-1}$ provided by Zhou (2001). This value will be used in our model calculations in the next section. However, the data may not be distributed as Gaussian random noise and more data points need to be collected to confirm this period change.

Since the modulation frequency $f_m = f_1 - f_0$ has not been varying significantly comparing to f_1 (Pócs & Szeidl 2001), one may take the method which used in Pócs & Szeidl (2001) and Zhou (2001) to calculate the rate of changes of the first overtone frequency. But the result show large uncertainties. Hence, we do not consider it a credible result from our observations.

5. CONSTRAINTS FROM THE THEORETICAL MODELS

Because the order of the period change of the fundamental mode is the same as the result from our calculation in Section 4 in the post-MS phase (about 10^{-8} yr^{-1}), then we assume that the result is completely from the evolutionary effects.

In this section, we describe the details of calculation of the theoretical models of AE UMa to constrain the physical parameters for the target. Subsection 5.1 presents the initial input physical parameters of AE UMa for the theoretical models, Subsection 5.2 uses the two frequencies f_0 and f_1 to constrain the initial parameters and determines some parameters for the subsequent calculation; Subsection 5.3 uses two independent ways to calculate the period changes of the fundamental mode of AE UMa induced by the stellar evolutionary effects.

5.1. Physical Parameters

Rodriguez et al. (1992) made *uvby* β photoelectric photometry for AE UMa. Intrinsic values of $b - y$, m_1 and c_1 were derived and the stellar physical parameters were determined. The effective temperature of AE UMa varied from 8320 K to 7150 K. The surface gravity $\log g$ varied from 4.16 to 3.77. The mean values obtained along the cycle were $\langle T_{\text{eff}} \rangle = 7560$ K and $\langle \log g \rangle = 3.90$, respectively. The metal abundance was estimated from δm_1 at the minimum light as $[Fe/H] = -0.3$. By using the $\log g - \log P$ relation derived by Claret et al. (1990), Rodriguez et al. (1992)

Table 7—Continued

NO.	T_{max}	E	$O - C$	Det	S	NO.	T_{max}	E	$O - C$	Det	S
406	55608.2954	157477	0.001969	CCD	(26)	431	55967.4159	161652	0.001098	CCD	(26)
407	55608.3763	157478	-0.003148	CCD	(26)	432	55968.2773	161662	0.002327	CCD	(26)
408	55610.3591	157501	0.001258	CCD	(26)	433	55968.3582	161663	-0.002790	CCD	(26)
409	55611.3877	157513	-0.002347	CCD	(26)	434	55969.3038	161674	-0.003379	CCD	(26)
410	55612.2469	157523	-0.003318	CCD	(26)	435	55969.3959	161675	0.002704	CCD	(26)
411	55612.3392	157524	0.002965	CCD	(26)	436	55997.0080	161996	0.003317	CCD	(26)
412	55613.1980	157534	0.001594	CCD	(26)	437	55997.0906	161997	-0.000100	CCD	(26)
413	55616.9800	157578	-0.001158	CCD	(26)	438	55997.1730	161998	-0.003717	CCD	(26)
414	55617.0705	157579	0.003325	CCD	(26)	439	55997.2639	161999	0.001166	CCD	(26)
415	55617.1520	157580	-0.001192	CCD	(26)	440	55998.0337	162008	-0.003188	CCD	(26)
416	55617.2358	157581	-0.003409	CCD	(26)	441	55998.1221	162009	-0.000805	CCD	(26)
417	55617.3281	157582	0.002874	CCD	(26)	442	55998.2119	162010	0.002977	CCD	(26)
418	55620.0772	157614	-0.000573	CCD	(26)	443	55998.2927	162011	-0.002240	CCD	(26)
419	55620.1602	157615	-0.003590	CCD	(26)	444	55998.9808	162019	-0.002276	CCD	(26)
420	55621.1103	157626	0.000322	CCD	(26)	445	55999.0727	162020	0.003606	CCD	(26)
421	55621.1986	157627	0.002604	CCD	(26)	446	55999.1547	162021	-0.000411	CCD	(26)
422	55937.3981	161303	0.003264	CCD	(26)	447	55999.2375	162022	-0.003628	CCD	(26)
423	55961.3051	161581	-0.002489	CCD	(26)	448	56000.0161	162031	0.000818	CCD	(26)
424	55961.3907	161582	-0.002906	CCD	(26)	449	56000.0978	162032	-0.003499	CCD	(26)
425	55964.3148	161616	-0.003387	CCD	(26)	450	56000.1874	162033	0.000084	CCD	(26)
451	56000.2762	162034	0.002867	CCD	(26)	457	56063.0691	162764	0.003287	CCD	(26)
452	56001.0459	162043	-0.001587	CCD	(26)	458	56064.0137	162775	0.001699	CCD	(26)
453	56001.1368	162044	0.003296	CCD	(26)	459	56064.0948	162776	-0.003218	CCD	(26)
454	56001.2186	162045	-0.000921	CCD	(26)	460	56065.0419	162787	-0.002306	CCD	(26)
455	56001.3023	162046	-0.003238	CCD	(26)	461	56068.0580	162822	0.003196	CCD	(26)
456	56062.0312	162752	-0.002407	CCD	(26)						

Note. — Source: (1) Tsesevich (1973); (2) Filatov (1960); (3) Pócs & Szeidl (2001); (4) Broglia & Conconi (1975); (5) Braune et al. (1979); (6) Braune & Mundry (1982); (7) Huebscher et al. (1985); (8) Rodriguez et al. (1992); (9) Hübscher et al. (1992); (10) Hintz et al. (1997a); (11) Agerer et al. (1999b); (12) Agerer et al. (1999a); (13) Pejcha et al. (2001); (14) Zhou (2001); (15) Agerer & Hubscher (2003); (16) Hubscher (2005); (17) Hubscher et al. (2005); (18) Klingenberg et al. (2006); (19) Hubscher et al. (2006); (20) Hubscher & Walter (2007); (21) Samolyk (2010); (22) Hubscher (2007); (23) Hubscher et al. (2009); (24) Hubscher et al. (2010); (25) Huebscher & Monninger (2011); (26) this work.

obtained the values of $M = 1.80 M_{\odot}$, $Age = 1.3 \times 10^9$ yr and $M_{bol} = 1^m.76$. Hintz et al. (1997a) provided the value of $[Fe/H] = -0.1$ according to the relation between the P_1/P_0 ratio and the $[Fe/H]$ value for dwarf Cepheids which was derived from Hintz et al. (1997b). They got the $[Fe/H]$ values ranging from -0.4 to -0.1 . We listed the parameters of AE UMa from Rodriguez et al. (1992) and Hintz et al. (1997a) in Table 8. The atmospheric parameters derived from our spectrum are in good agreement with that above values, in particular for the metal ratio $[Fe/H]$ (comparison of Table 3 to 11). We note that, in order to perform a search for the best fitting model in a wide parametric range, we used 3σ as the intervals of constraints for our theoretical calculation as follows.

5.2. Constraints from f_0 and f_1

Modules for Experiments in Stellar Astrophysics (MESA) is a suite of source-open, robust, efficient, thread-safe libraries for a wide range of applications in computational stellar astrophysics (Paxton et al. 2011, 2013). The 1-D stellar evolution module, MESA star, combines many of the numerical and physics modules for simulations of a wide range of stellar evolution scenarios ranging from very-low mass to massive stars, including advanced evolutionary phases. The "astero" extension to MESA star implements an integrated approach that passes results automatically between MESA star and the new MESA module based on the adiabatic code ADIPLS (Christensen-Dalsgaard 2008).

In MESA version 6208, the *astero* extension enables calculation of selected pulsation frequencies by MESA star during the evolution of the model. This allows fitting to the observations that can include spectroscopic constraints (e.g., $[Fe/H]$, $\log g$ and T_{eff}), asteroseismic constraints, the large frequency separation ($\Delta\nu$) and the frequency of maximum power (ν_{max}), and even individual frequencies observed. For the automated χ^2 minimization, *astero* will evolve a pre-main sequence model from a user defined starting point, and find the best match along that single evolutionary track. The code then recalculates the track, again initiated at the pre-main sequence, with different initial parameters such as mass, chemical composition, mixing length parameter and overshooting,

Table 8: Physical parameters of AE UMa from Rodriguez et al. (1992) and Hintz et al. (1997a). The $\log(L/L_{\odot})$ value was derived based on $\log(L/L_{\odot}) = 0.4(M_{bol_{\odot}} - M_{bol})$.

Parameters	Mean value	Intervals	3σ
$[Fe/H]$	-0.3	[-0.4,-0.1]	—
T_{eff} (K)	7569	[7150,8320]	[5980,9490]
$\log g$	3.90	[3.77,4.16]	[3.38,4.55]
M_{bol}	—	[1.53,1.93]	[1.33,2.13]
$M(M_{\odot})$	—	[1.75,1.95]	—
$\log(L/L_{\odot})$	—	[1.16,1.32]	[1.08,1.40]

and repeats until the minimum χ^2 is found.

We used the scan-grid mode to minimize the χ^2 for each model, which helps to compact the intervals of the physical parameters.

Every model of evolution starts with creating a pre-main-sequence model by specifying the mass, M , at a uniform composition. The equation-of-state tables are constructed from the 2005 update of the OPAL EOS tables (Rogers & Nayfonov 2002) and SCVH tables (Saumon et al. 1995). The MESA opacity tables, which are derived from Type 1 and 2 OPAL tables (Iglesias & Rogers 1993, 1996), tables from OP Seaton (2005), and Ferguson et al. (2005), cover a large range $2.7 \leq \log T \leq 10.3$ and $-8 \leq \log R \leq 8$. The hydrogen burning reaction rates in the calculations are from Bahcall (1997, 2002).

MESA star treats convective mixing as a time-dependent, diffusive process with a diffusion coefficient D as

$$D_{OV} = D_{conv,0} \exp\left(-\frac{2z}{f\lambda_{P,0}}\right), \quad (5)$$

where $\lambda_{P,0}$ is the pressure scale height at that location, z is the distance in the radiative layer away from that location, and f is an adjustable parameter (Herwig 2000).

In all our subsequent calculation, the used opacity and EOS tables are *eos_file_prefix = mesa*, *kappa_file_prefix = gs98* and *kappa_lowT_prefix = lowT_Freedman11*. The atmosphere model is *which_atm_option = photosphere_tables* photosphere.

The mixing-length parameter α_{MLT} was chosen as 1.89, since the choice has actually a very small effect on our models (Yang et al. 2012). The convective overshooting parameter $f_{ov} = 0.015$ was the initial value of MESA (version 6208). The effects of rotation on the evolutionary period changes are disregarded, concerning AE UMa as a HADS which are very slow rotators (Breger 2000). Table 9 lists the parameters of the grid of model to search for f_0 and f_1 of AE UMa. The diffusion effects were not taken into account because of its negligible results on the models with mass $1.30 M_{\odot}$ to $2.70 M_{\odot}$ after the main sequence and the post-main sequence (before Red Giant phase).

As the result, we got the models which included the frequencies f_0 and f_1 along with the stellar evolution tracks. These tracks provided the relevant intervals of the parameters for subsequent calculation, as listed in Table 10.

With the observations and the method used, one can believe that $[Fe/H]$ and $\log g$ values are in good reliability (Strömberg 1956; Crawford & Mander 1966). So, we decide to take the value $[Fe/H] = -0.3$ in our calculation.

We used the formula (with the solar metallicity $X_{\odot} = 0.7381$, $Y_{\odot} = 0.2485$ and $Z_{\odot} = 0.0134$ from Asplund et al. (2009)),

$$[Fe/H] = \log\left(\frac{Z}{X}\right) - \log\left(\frac{Z_{\odot}}{X_{\odot}}\right) \quad (6)$$

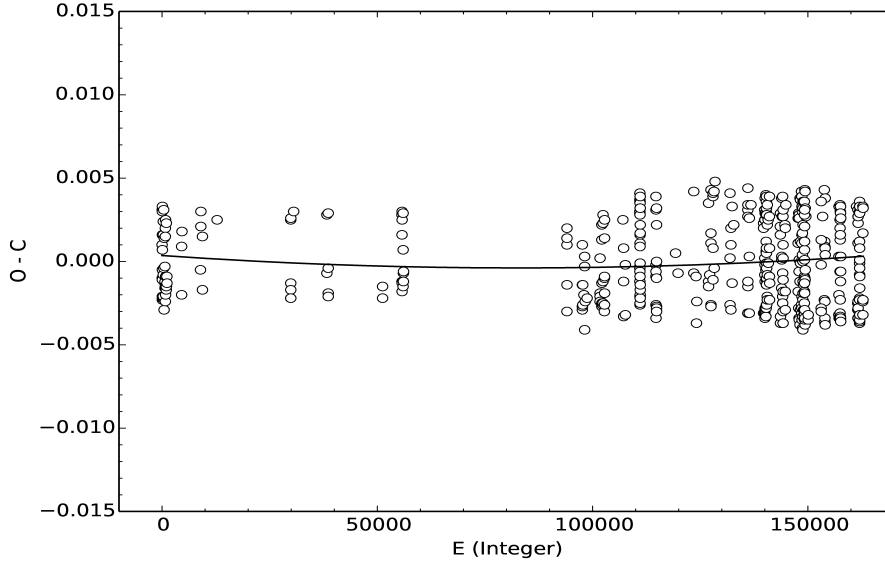


Fig. 6.— $O - C$ diagram of AE UMa. The $O - C$ values are in *days*. E is the cycle number. The solid curve shows the fit concerning a continuous increasing period change.

Table 9: The parameters of the grid of model to search for f_0 and f_1 . Since the values of M_{bol} and $\log(L/L_{\odot})$ in Table 6 were calculated from the stellar models Rodriguez et al. (1992) other than from observations, which depended on the models they used, we did not use these values as the constraints during our calculation.

Parameters	Maximum	Minimum	Step
$[Fe/H]$	-0.1	-0.4	0.05
initial Y	0.33	0.23	0.02
Mass	2.7	1.3	0.02
$\log T_{eff}$	3.977	3.777	—
$\log g$	4.55	3.38	—

Table 10: The parameters determined with the constraints from f_0 and f_1 . The grid was constructed also within the parameters intervals of T_{eff} and $\log g$ listed in Table 6. In order to show an obvious comparison of the evolutionary tracks, we calculated the tracks with the stellar mass from 1.30 to $2.30M_{\odot}$.

Parameters	Maximum	Minimum
$[Fe/H]$	-0.2	-0.4
initial Y	0.27	0.23
Mass	2.26	1.32

and the formula,

$$X + Y + Z = 1 \tag{7}$$

to calculate the initial Z . In Girardi et al. (2000), a model was calculated with a couple of value $(Y, Z) = (0.25, 0.008)$, which accords with the values in our previous calculation (derived with MESA *astero* with the value of $[Fe/H]$).

At last, by integrating all the information about the value of (Y, Z) , we decide to choose $(Y, Z) = (0.25, 0.008521)$ as the unique initial value for the subsequent calculation.

5.3. Constraints from the Period Variation

Not like the solar-like stars for which many frequencies are detected, most HADS are observed with only the fundamental and the first overtone modes in general (e.g., Balona et al. 2012; Ulusoy et al. 2013). As a result, the period variation becomes a very important constraint on the model calculation of these stars. Detection of high precision of period variation may offer strong constraints on AE UMa. We used two independent ways to calculate the period variations of AE UMa theoretically.

5.3.1. Calculation from Stellar Evolutionary Effect

The variation rate of the fundamental period derived from long time-scale of observations of AE UMa shows a positive period change. From the theoretical point of view, the period changes caused by stellar evolution in and across the lower instability strip permit an observational test of stellar evolution theory (Breger & Pamyatnykh 1998).

The period-luminosity-color relation can be expressed as (Breger & Pamyatnykh 1998)

$$\log P = -0.3M_{bol} - 3 \log T_{eff} - 0.5 \log M + \log Q + constant, \tag{8}$$

where P is the period of a radial mode of pulsation, M_{bol} is the bolometric absolute magnitude, T_{eff} is the effective temperature, M is the stellar mass in solar mass, and Q is the pulsation constant in days. For δ Scuti stars with radial pulsation, the constant is 12.708. For individual stars, evolutionary period changes over long time scales. An evolutionary change in T_{eff} , M_{bol} , and M leads to a period change of

$$\frac{1}{P} \frac{dP}{dt} = -0.69 \frac{dM_{bol}}{dt} - \frac{3}{T_{eff}} - 0.5 \frac{1}{M} \frac{dM}{dt} + \frac{1}{Q} \frac{dQ}{dt}. \tag{9}$$

Assuming that the stellar mass $M = constant$ for δ Scuti stars during the observation interval with mass of $1.30 - 2.30 M_{\odot}$ and that the variation of pulsation constant is negligible as a very

small quantity, Yang et al. (2012) got,

$$\frac{1}{P} \frac{dP}{dt} \approx -0.69 \frac{dM_{bol}}{dt} - \frac{3}{T_{eff}} \frac{dT_{eff}}{dt}. \quad (10)$$

As indicated by Rodríguez & Breger (2001), the HADS locate on or near the main sequence of the H-R diagram. Consequently, the evolutionary models are constructed from the pre-main-sequence Hayashi phase to the end of the main sequence. The effect of rotation was not considered here for mainly two reasons: (1) the HADS stars are typically with slow rotation and most have a projected rotational velocity, $V \sin i$, around 20 km s⁻¹ (see, e.g., Solano & Fernley 1997); (2) the effects of rotation with speed of $V \sin i = 18$ km s⁻¹ in HADS is very similar to that of absence of rotation (Casas et al. 2006).

The evolutionary tracks we constructed from 1.30 M_{\odot} to 2.30 M_{\odot} are shown in Figure 7, and the corresponding variation rates of the period are marked.

As shown in Figure 7, the states whose values of period changes are consistent with the observed ones determined from the $O - C$ analysis lie just after the second turn-offs leaving the main sequences on the evolutionary tracks.

5.3.2. Calculation from ADIPLS

ADIPLS (the Aarhus adiabatic oscillation package) is a progame for calculation of adiabatic oscillations of stellar models (Christensen-Dalsgaard 2008). We used it to calculate the frequencies of the eigen modes of the model at each step of our evolutionary state. As a result, we got the frequencies of the model of F_0 and F_1 then deduced the variation of the frequencies of F_0 and F_1 . In the calculation, the input frequencies F_0 and F_1 are the fundamental and first overtone frequencies with quantum numbers of $l = 0$ and $n = 1, 2$, respectively.

We calculated the evolutionary tracks from 1.30 M_{\odot} to 2.30 M_{\odot} , and got the frequency values on each tracks, as shown in Figure 8. Figure 8 (a) and (b) show that the models with appropriate frequencies for AE UMa could appear (i) just before the first turn-offs, (ii) after the first and before the second turn-offs, (iii) just after the second turn-offs. We integrated the constraints from f_0 and f_1 and got the results shown in Figure 8 (c).

In addition, we also calculated the variations of the frequencies of the eigen-modes of the models by using ADIPLS. Adding the constraint from $(1/P_0)(dP_0/dt)$ which are thought to be due to the evolutionary effects, we got the results in Figure 9.

One can find that this result is almost consistent with the result from Figure 7 just after the second turn-off. The differences come from we did not consider the variation of the stellar mass and the pulsation constant along the evolutionary tracks in Figure 7.

Finally, we combined the constraints from f_0 , f_1 and $(1/P_0)(dP_0/dt)$, and got the results which

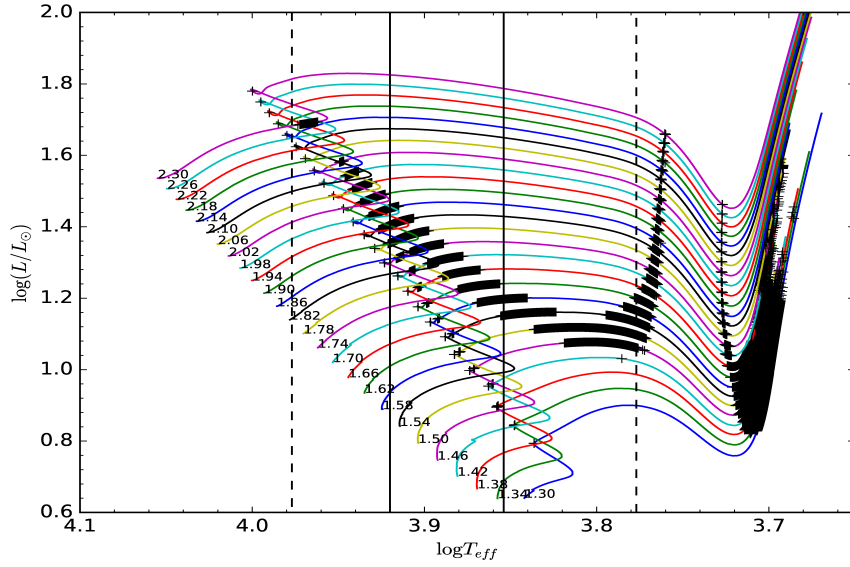
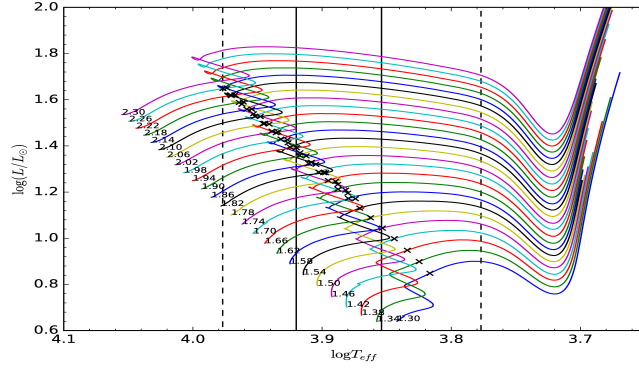
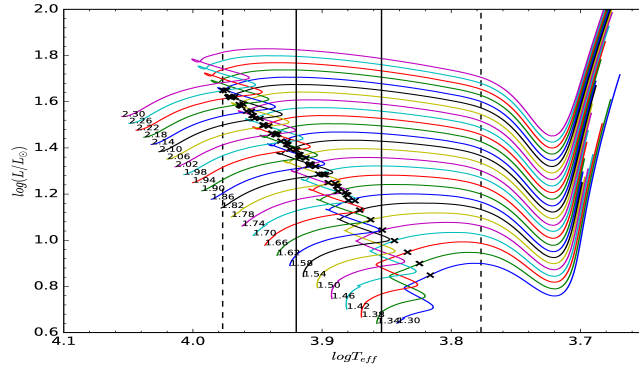


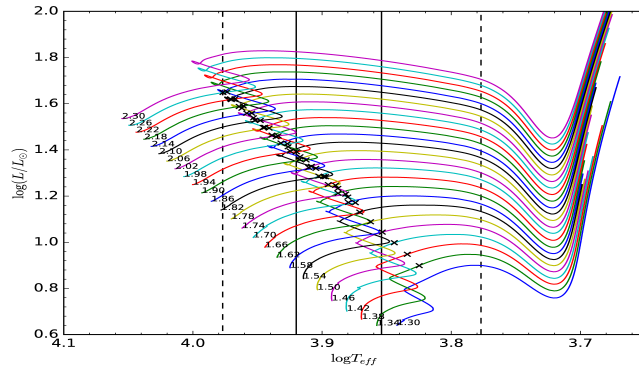
Fig. 7.— Evolutionary tracks of models with mass from $1.30 M_{\odot}$ to $2.30 M_{\odot}$ for $(Y, Z) = (0.25, 0.008521)$. The solid and dashed vertical lines on the H-R diagram are determined from the observed T_{eff} in 1σ and 3σ , respectively. The Marks on the tracks indicate the models with the values of the evolutionary period changes of $(1/P_0)(dP_0/dt)$ inside the interval $[3.5210 \times 10^{-9}, 7.2448 \times 10^{-9}]$ in units of yr^{-1} . Please note that, the tracks are shown on the diagram with the mass interval of $0.04M_{\odot}$.



(a)



(b)



(c)

Fig. 8.— Models with the values of F_0 and F_1 calculated from ADIPLS consistent with the observed ones ($F_0 \in [f_0 - 3\sigma, f_0 + 3\sigma]$ and $F_1 \in [f_1 - 3\sigma, f_1 + 3\sigma]$) are marked on the evolutionary tracks. (a): for $F_0 \in [f_0 - 3\sigma, f_0 + 3\sigma]$; (b): for $F_1 \in [f_1 - 3\sigma, f_1 + 3\sigma]$; (c): for both $F_0 \in [f_0 - 3\sigma, f_0 + 3\sigma]$ and $F_1 \in [f_1 - 3\sigma, f_1 + 3\sigma]$.

is shown in Figure 10.

One concludes that AE UMa should locate after the second turn-offs of the evolutionary tracks leaving the MS. Hence, one finds that the period variations of the fundamental mode of AE UMa are caused by the evolutionary effect. The rate of variation is consistent with the theoretically predicted value by Breger & Pamyatnykh (1998).

With the discussion above and constraints from the physical parameters, one can conclude that the mass of AE UMa ranges from $1.75 M_{\odot}$ to $1.86 M_{\odot}$, the age from 0.96×10^9 yr to 1.15×10^9 yr.

We chose $1.80 M_{\odot}$ as a sample to study the evolutionary state and the interior of the models that we gained. More details of the parameters we got from calculation are listed in Table 11. Figure 11 shows the distribution of H , He^3 and He^4 versus the stellar radius. Figure 12 presents the energy distribution inside the star. From Figure 11 and 12, one may find that the star should have a helium core and a hydrogen-burning shell.

We also calculated models with different values of Y , Z and α_{ov} by using different grids. The result showed that the states were not different significantly. All the results pointed out that AE UMa should lie just after the second turn-off with a helium core and a hydrogen-burning shell.

6. CONCLUSIONS

We analyse the photometric data gathered on AE UMa with 40 nights spanning over from 2009 to 2012 and detect 37 frequencies above the so-called 4σ detection threshold, among which 25 frequencies are newly detected. All these frequencies are linked to be either harmonics or linear combinations of the two main frequencies $f_0 = 11.62560 \text{ c d}^{-1}$ and $f_1 = 15.03123 \text{ c d}^{-1}$, corresponding to the fundamental and the first overtone radial pulsation modes, respectively. No frequencies of the other pulsation modes were detected from the observed data.

An $O - C$ diagram is constructed with combination of the 84 times of maximum light determined from our new observations and 360 ones listed in the literature, leading to the updated value of period $P_0 = 0.0860170781$ days. A new ephemeris with a quadratic solution suggests that the

Table 11: Physical parameters of AE UMa obtained from our calculation.

Parameter	Value	Uncertainty (%)
Mass (M_{\odot})	1.805 ± 0.055	3.04
Age (10^9 yr)	1.055 ± 0.095	9.00
$\log T_{\text{eff}}$	3.922 ± 0.01	0.25
Radius (10^{11} cm)	1.647 ± 0.032	1.94
$\log g$	3.9543 ± 0.0044	0.11
$\log L$	1.381 ± 0.048	3.51

period change rate of the fundamental mode of AE UMa is of $(1/P_0)(dP_0/dt) = 5.4(\pm 1.9) \times 10^{-9} \text{ yr}^{-1}$. The value is different with the result obtained by Zhou (2001) and need to be confirmed with more data that will be collected from observations in the near future, both from ground and space (e.g., TESS, Ricker et al. 2014). Because the large values of the derivative of $(1/P_1)(dP_1/dt)$ obtained from the standard $O - C$ method, we did not use this value as a constraint in the model calculation.

With the spectroscopic observation data, we got the low-resolution spectrum and used the automated 1D parametrization pipeline LASP to obtain the stellar atmospheric parameters of AE UMa. These parameters (especially the $[Fe/H]$ value of -0.32) certificate that AE UMa is a Pop. I δ Scuti star rather than a Pop. II SX Phe star.

We then calculated models of stars with masses between $1.30 M_\odot$ and $2.70 M_\odot$. With the constraints of the values of f_0 , f_1 and $(1/P_0)(dP_0/dt)$, we conclude that AE UMa lies just after the second turn-offs of the evolutionary tracks leaving the main sequence. The corresponding mass should be $1.805 \pm 0.055 M_\odot$ and the age $1.055 \pm 0.095 \times 10^9 \text{ yr}$. At this evolutionary phase, the star should have a helium core and a hydrogen-burning shell.

Moreover, according to the concrete observational evidence, we provide an example of the HADS whose evolutionary stage is on the post-main-sequence. This gives a direct support to the general consensus that δ Scuti stars are probably normal stars evolving in the main-sequence or the immediate post-main-sequence stages.

Acknowledgments

JSN and JNF acknowledge the support from the Joint Fund of Astronomy of National Natural Science Foundation of China (NSFC) and Chinese Academy of Sciences through the grant U1231202, the NSFC grant 11673003, the National Basic Research Program of China (973 Program 2014CB845700 and 2013CB834900), and the LAMOST FELLOWSHIP supported by Special Funding for Advanced Users, budgeted and administrated by Center for Astronomical Mega-Science, Chinese Academy of Sciences (CAMS). JSN thanks Nami Mowlavi for helpful discussions and useful advice.

REFERENCES

- Agerer, F., Dahm, M., & Hubscher, J. 1999a, Information Bulletin on Variable Stars, 4712, 1
- Agerer, F., Dahm, M., & Hubscher, J. 1999b, Information Bulletin on Variable Stars, 4712, 1
- Agerer, F. & Hubscher, J. 2003, Information Bulletin on Variable Stars, 5485, 1
- Asplund, M., Grevesse, N., Sauval, A. J., & Scott, P. 2009, ARA&A, 47, 481

- Baglin, A., Breger, M., Chevalier, C., et al. 1973, *A&A*, 23, 221
- Bahcall, J. N. 1997, *Phys. Rev. C*, 56, 3391
- Bahcall, J. N. 2002, *Phys. Rev. C*, 65, 025801
- Balona, L. A., Lenz, P., Antoci, V., et al. 2012, *MNRAS*, 419, 3028
- Braune, W., Huebscher, J., & Mundry, E. 1979, *Astronomische Nachrichten*, 300, 165
- Braune, W. & Mundry, E. 1982, *Berliner Arbeitsgemeinschaft fuer Veraenderliche Sterne - Mitteilungen*, 34
- Breger, M. 1979, *PASP*, 91, 5
- Breger, M. 1980, *ApJ*, 235, 153
- Breger, M. 2000, in *Astronomical Society of the Pacific Conference Series*, Vol. 210, *Delta Scuti and Related Stars*, ed. M. Breger & M. Montgomery, 3
- Breger, M. & Pamyatnykh, A. A. 1998, *A&A*, 332, 958
- Breger, M., Stich, J., Garrido, R., et al. 1993, *A&A*, 271, 482
- Brogia, P. & Conconi, P. 1975, *A&AS*, 22, 243
- Casas, R., Suárez, J. C., Moya, A., & Garrido, R. 2006, *A&A*, 455, 1019
- Christensen-Dalsgaard, J. 2008, *Ap&SS*, 316, 113
- Claret, A., Rodriguez, E., Rolland, A., & Lopez de Coca, P. 1990, in *Astronomical Society of the Pacific Conference Series*, Vol. 11, *Confrontation Between Stellar Pulsation and Evolution*, ed. C. Cacciari & G. Clementini, 481
- Crawford, D. L. & Mander, J. 1966, *AJ*, 71, 114
- Ferguson, J. W., Alexander, D. R., Allard, F., et al. 2005, *ApJ*, 623, 585
- Filatov, G. S. 1960, *Astronomicheskij Tsirkulyar*, 215, 20
- Fu, J. N., Khokhuntod, P., Rodríguez, E., et al. 2008a, *AJ*, 135, 1958
- Fu, J.-N., Zhang, C., Marak, K., et al. 2008b, *Chinese J. Astron. Astrophys.*, 8, 237
- Garcia, J. R., Cebral, J. R., Scoccimarro, E. R., et al. 1995, *A&AS*, 109, 201
- Geyer, E., Kippenhahn, R., & Strohmeier, W. 1955, *Kleine Veröff, Bamberg*, 11
- Girardi, L., Bressan, A., Bertelli, G., & Chiosi, C. 2000, *A&AS*, 141, 371

- Götz, W. & Wenzel, W. 1961, Sonneberg, 571
- Herwig, F. 2000, A&A, 360, 952
- Hintz, E., Hintz, M. L., & Joner, M. D. 1997a, PASP, 109, 1073
- Hintz, E. G., Joner, M. D., McNamara, D. H., et al. 1997b, PASP, 109, 15
- Hubscher, J. 2005, Information Bulletin on Variable Stars, 5643, 1
- Hubscher, J. 2007, Information Bulletin on Variable Stars, 5802, 1
- Hübscher, J., Agerer, F., & Wunder, E. 1992, Berliner Arbeitsgemeinschaft fuer Veraenderliche Sterne - Mitteilungen, 60, 1
- Hubscher, J., Lehmann, P. B., Monninger, G., Steinbach, H.-M., & Walter, F. 2010, Information Bulletin on Variable Stars, 5918, 1
- Hubscher, J., Paschke, A., & Walter, F. 2005, Information Bulletin on Variable Stars, 5657, 1
- Hubscher, J., Paschke, A., & Walter, F. 2006, Information Bulletin on Variable Stars, 5731, 1
- Hubscher, J., Steinbach, H.-M., & Walter, F. 2009, Information Bulletin on Variable Stars, 5874, 1
- Hubscher, J. & Walter, F. 2007, Information Bulletin on Variable Stars, 5761, 1
- Huebscher, J., Lichtenknecker, D., & Mundry, E. 1985, Berliner Arbeitsgemeinschaft fuer Veraenderliche Sterne - Mitteilungen, 39
- Huebscher, J. & Monninger, G. 2011, Berliner Arbeitsgemeinschaft fuer Veraenderliche Sterne - Mitteilungen, 214, 1
- Iglesias, C. A. & Rogers, F. J. 1993, ApJ, 412, 752
- Iglesias, C. A. & Rogers, F. J. 1996, ApJ, 464, 943
- Kepler, S. O., Castanheira, B. G., Saraiva, M. F. O., et al. 2005, A&A, 442, 629
- Klingenberg, G., Dvorak, S. W., & Robertson, C. W. 2006, Information Bulletin on Variable Stars, 5701, 1
- Lenz, P. & Breger, M. 2005, Communications in Asteroseismology, 146, 53
- Niu, J.-S., Fu, J.-N., & Zong, W.-K. 2013, Research in Astronomy and Astrophysics, 13, 1181
- Paxton, B., Bildsten, L., Dotter, A., et al. 2011, ApJS, 192, 3
- Paxton, B., Cantiello, M., Arras, P., et al. 2013, ArXiv e-prints
- Pejcha, O., Havlik, T., & Kral, L. 2001, Information Bulletin on Variable Stars, 5080, 1

- Petersen, J. O. & Christensen-Dalsgaard, J. 1996, *A&A*, 312, 463
- Pócs, M. D. & Szeidl, B. 2001, *A&A*, 368, 880
- Poretti, E. 2003, *A&A*, 409, 1031
- Pringle, J. E. 1975, *MNRAS*, 170, 633
- Ricker, G. R., Winn, J. N., Vanderspek, R., et al. 2014, in *Proc. SPIE, Vol. 9143, Space Telescopes and Instrumentation 2014: Optical, Infrared, and Millimeter Wave*, 914320
- Rodríguez, E. & Breger, M. 2001, *A&A*, 366, 178
- Rodríguez, E. & López-González, M. J. 2000, *A&A*, 359, 597
- Rodríguez, E., Rolland, A., Lopez de Coca, P., Garcia-Lobo, E., & Sedano, J. L. 1992, *A&AS*, 93, 189
- Rogers, F. J. & Nayfonov, A. 2002, *ApJ*, 576, 1064
- Samolyk, G. 2010, *Journal of the American Association of Variable Star Observers (JAAVSO)*, 38, 12
- Saumon, D., Chabrier, G., & van Horn, H. M. 1995, *ApJS*, 99, 713
- Seaton, M. J. 2005, *MNRAS*, 362, L1
- Solano, E. & Fernley, J. 1997, *A&AS*, 122
- Strömgren, B. 1956, *Vistas in Astronomy*, 2, 1336
- Szeidl, B. 1974, *Information Bulletin on Variable Stars*, 903, 1
- Tsesevich, V. P. 1973, *Astronomicheskij Tsirkulyar*, 775, 2
- Ulusoy, C., Ulaş, B., Gülmez, T., et al. 2013, *MNRAS*, 433, 394
- Wenger, M., Ochsenbein, F., Egret, D., et al. 2000, *A&AS*, 143, 9
- Wu, Y., Luo, A.-L., Li, H.-N., et al. 2011, *Research in Astronomy and Astrophysics*, 11, 924
- Yang, X. H., Fu, J. N., & Zha, Q. 2012, *AJ*, 144, 92
- Zhou, A.-Y. 2001, *A&A*, 374, 235
- Zhou, A.-Y., Jiang, X.-J., Zhang, Y.-P., & Wei, J.-Y. 2009, *Research in Astronomy and Astrophysics*, 9, 349
- Zong, W., Fu, J.-N., Niu, J.-S., et al. 2015, *AJ*, 149, 84

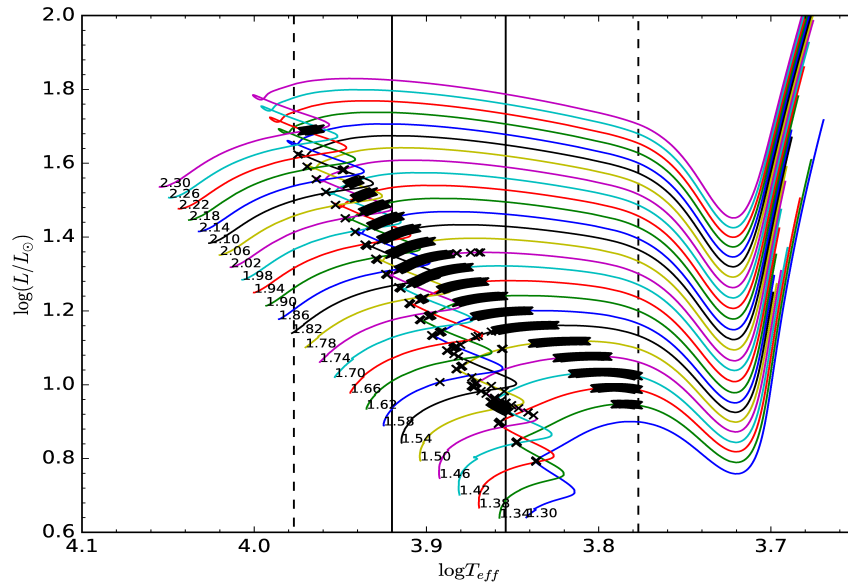
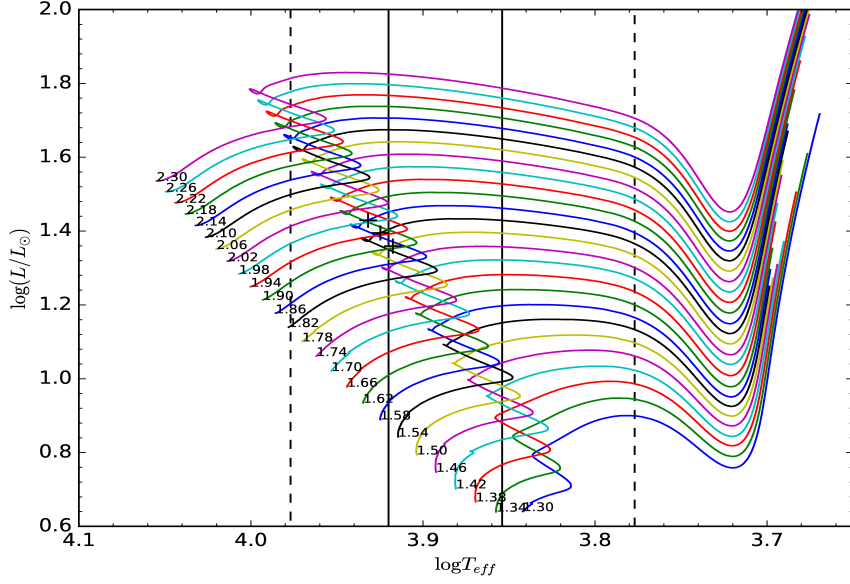
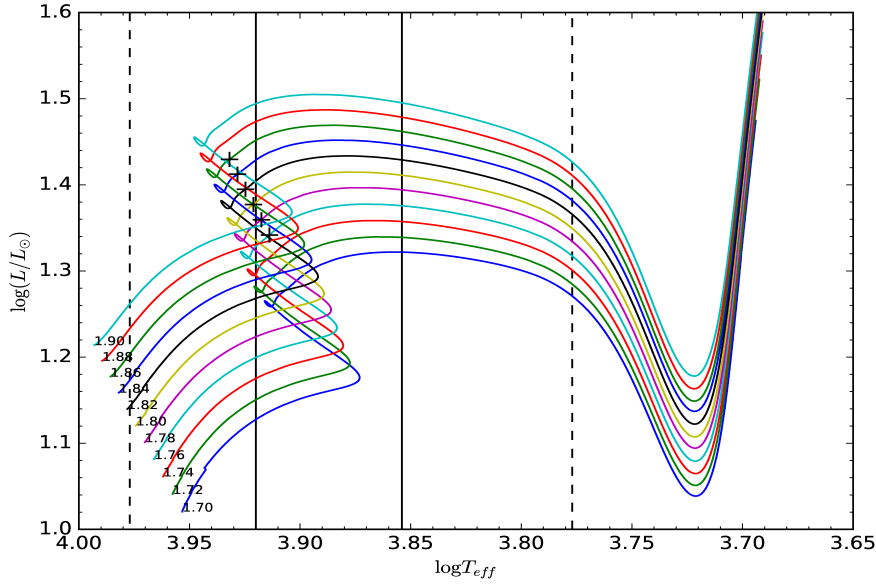


Fig. 9.— The models for which the period variations of the fundamental mode $(1/P_0)(dP_0/dt)$ calculated with ADIPLS agree with the observed values of $5.3829(\pm 1.8619) \times 10^{-9} \text{ yr}^{-1}$ are marked on the evolutionary tracks.



(a)



(b)

Fig. 10.— Evolutionary tracks of star models. (a): marks on the tracks indicate the models with constraints from f_0 , f_1 and $(1/P_0)(dP_0/dt)$. (b): A zoom in of the (a).

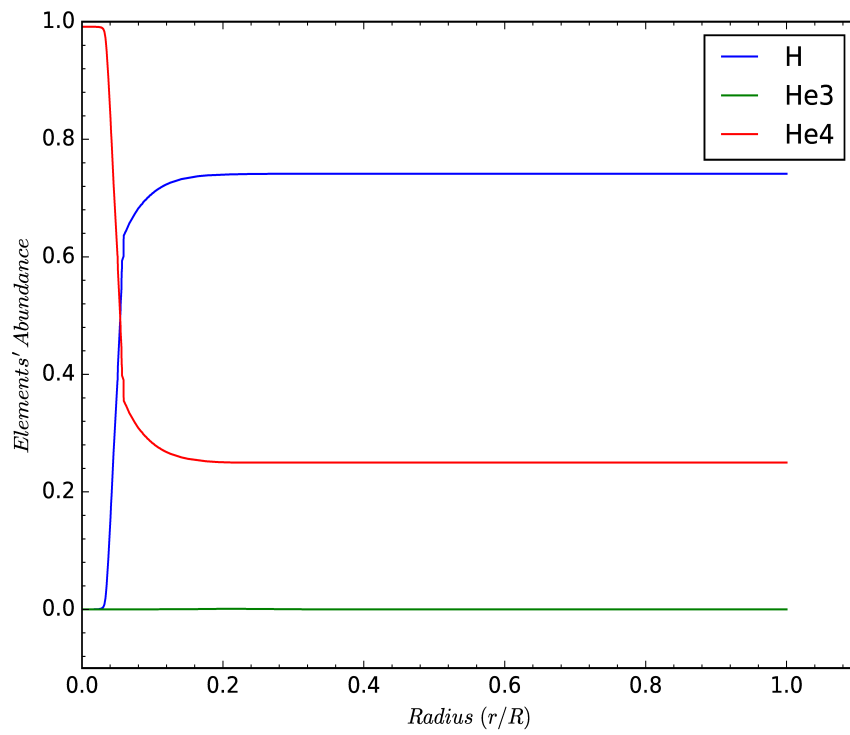


Fig. 11.— Elements' Abundance distribution of H , He^3 and He^4 inside the star for the model with the star mass of $1.80M_{\odot}$.

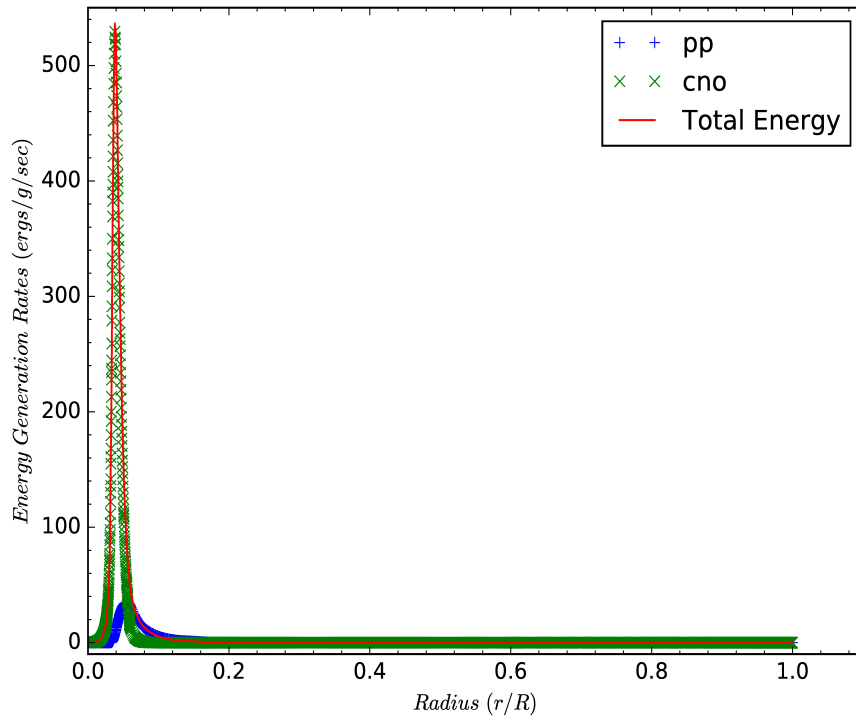


Fig. 12.— Energy generation rates distribution inside the star for the model with the star mass of $1.80M_{\odot}$.